Mathematical Biology

Modelling of the activation of G-protein coupled receptors: drug free constitutive receptor activity

**P. J. Woodroffe · L. J. Bridge · J. R. King ·
C. Y. Chen · S. J. Hill**

Abstract G-protein coupled receptors (GPCRs) form a crucial component of approximately 80% of hormone pathways. In this paper, the most popular mechanism for activation of GPCRs—the shuttling mechanism—is modelled mathematically. An asymptotic analysis of this model clarifies the dynamics of the system in the absence of drug, in particular which reactions dominate during the different timescales. Equilibrium analysis of the model demonstrates the model's ability to predict constitutive receptor activity.

1 Introduction

1.1 Motivation

Since multicellular organisms first appeared on the earth, an essential factor in their success has been the effectiveness of communication between their component cells.

P. J. Woodroffe · L. J. Bridge (✉) · J. R. King
Centre for Mathematical Medicine, Division of Theoretical Mechanics,
School of Mathematical Sciences, University of Nottingham, Nottingham, UK
e-mail: lloyd.bridge@nottingham.ac.uk

C. Y. Chen
Department of Applied Mathematics, National University of Kaohsiung,
Kaohsiung, Taiwan

S. J. Hill
Institute of Cell Signalling, Medical School, Queen's Medical Centre, Nottingham, UK

Complex internal machinery is needed for the cells to coordinate their behaviour, allowing each individual cell to recognise its position and importance to the body as a whole: for example, having neighbouring cells control the rate of cell division is an important "social control". The breakdown of such a control can lead to cancer, probably killing the organism (Alberts et al. 1994).

One specific type of intercellular communication involves the use of *G-protein coupled receptors* (GPCRs). It has been estimated that as much as 5% of the human genome codes for these receptors and approximately 80% of all known hormones, neurotransmitters and neuromodulators act through them. In addition, it is believed that between 45 and 60% of all pharmaceuticals used today act through GPCRs (Riccobene et al. 1999; Woolf et al. 2001).

Examples of GPCR systems include the β_1-adrenoreceptor that adrenaline binds to, regulating heart contractility, and the opioid receptor, in the brain and spinal cord, to which opiates (such as morphine) can bind to suppress pain. Drugs called β-blockers have been developed which have been proven to be effective means of alleviating medical conditions such as hypertension and congestive heart failure, by antagonising the effects of endogenous hormones (Adams et al. 1998; Fitzgerald et al. 1999; Woolf et al. 2001). Thus, better understanding of the mechanisms of G-protein activation should lead to increased efficiency of existing treatments and could be instrumental in provoking developments that could lead to new drugs to combat currently uncurable diseases (Fitzgerald et al. 1999; Kenakin 1997).

1.2 Background

The GPCR signalling pathway is initiated by a ligand. Many different substances can act as ligands, including light, lipids, proteins, peptides, biogenic amines, nucleotides, drugs (Fitzgerald et al. 1999) and, most specifically, hormones. The ligand interacts with a responsive cell through a number of receptors on the cell's surface. Although there are many different GPCRs, the specific type of receptor in which we are interested, they all have the same basic structure. They consist of a single protein strand that passes through the lipid bilayer (which forms the cell surface) seven times. The extracellular part of the GPCR has a domain that accepts a specific ligand (see Fig. 1). The GPCR undergoes a conformational change on binding (expressed by K_P), opening a binding site *inside* the cell. This allows the GPCR to bind to the next player in the G-protein signalling game, the G-protein itself (expressed by K_G), this being a heterotrimeric (composed of three distinct parts) GTP-binding (binds to guanosine triphosphate) protein. The three parts are designated the α, β and γ components (see Fig. 2), each being encoded by a distinct gene. The G-protein α sub-units are divided into four main classes termed G_s, G_i, G_q and G_{12}, depending on their function (Watson and Arkinstall 1994). Each class stimulates/inhibits different internal enzymes.

The α subsection of the G-protein in Fig. 2 is bound to a molecule of guanine diphosphate (GDP). This is its "inactive" state. The heterotrimeric G-protein can interact with the ligand-bound receptor, forming a temporary complex. This triggers the dissociation of GDP from the G-protein, forming a transient "empty" state. From this state, either another molecule of GDP will bind (returning the G-protein to its inactive state)
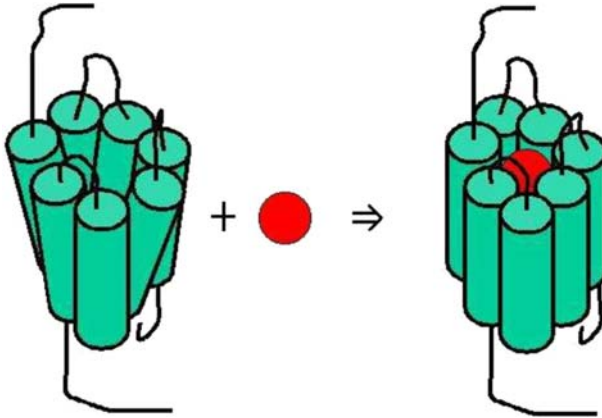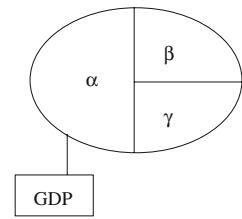
Fig. 1 Schematic of ligand binding to a GPCR. The top of the picture represents the extracellular region, the bottom the intracellular

Fig. 2 Schematic of an inactive heterotrimeric G-protein

or guanosine triphosphate (GTP) will bind, triggering a further conformational change (expressed by K_{act}) that causes the G-protein not only to dissociate from the GPCR but also to split up into G_α and $G_{\beta\gamma}$ units (the β and γ subunits forming a tight complex). These proceed to regulate effector activities. The G-protein is deactivated when the G_α-GTP subunit is hydrolysed back to G_α-GDP (expressed by K_{gtp}), which subsequently reassociates with $G_{\beta\gamma}$ (expressed by K_B) to produce the inactive G-protein (see Fig. 3 for a schematic of this process) (Alberts et al. 1994; Watson and Arkinstall 1994). The G_α-GTP subunit binds to effector enzymes (such as adenylyl cyclase) to continue the signalling pathway, however in this paper we will consider the concentration of the G_α-GTP subunit to be the measurable reponse. This mechanism, whereby the G_α-GTP subunit shuttles between its associated receptor and its target enzyme, is known as the *shuttling mechanism* (Shea et al. 2000) and is the most popular theory as to how a GPCR activates its associated effector enzyme. For example, the α subunit from the G_s-protein shuttles between the β_2-adrenergic receptor and adenylyl cyclase.

However, Fig. 3 is a simplification of the G-protein activation process, since G-proteins are also able to bind to a GPCR *before* a ligand has bound. This is called pre-coupling and the amount of pre-coupling depends on both the receptor and the G-protein. In this paper, the equilibrium constant K_G is the parameter that determines the amount of pre-coupling. Approximately 50% of the N-formyl peptide receptors in neutrophils and 30% of the α_2-adrenergic receptors in platelet membranes are thought to be pre-coupled (Shea et al. 2000). These pre-coupled complexes are not active, but
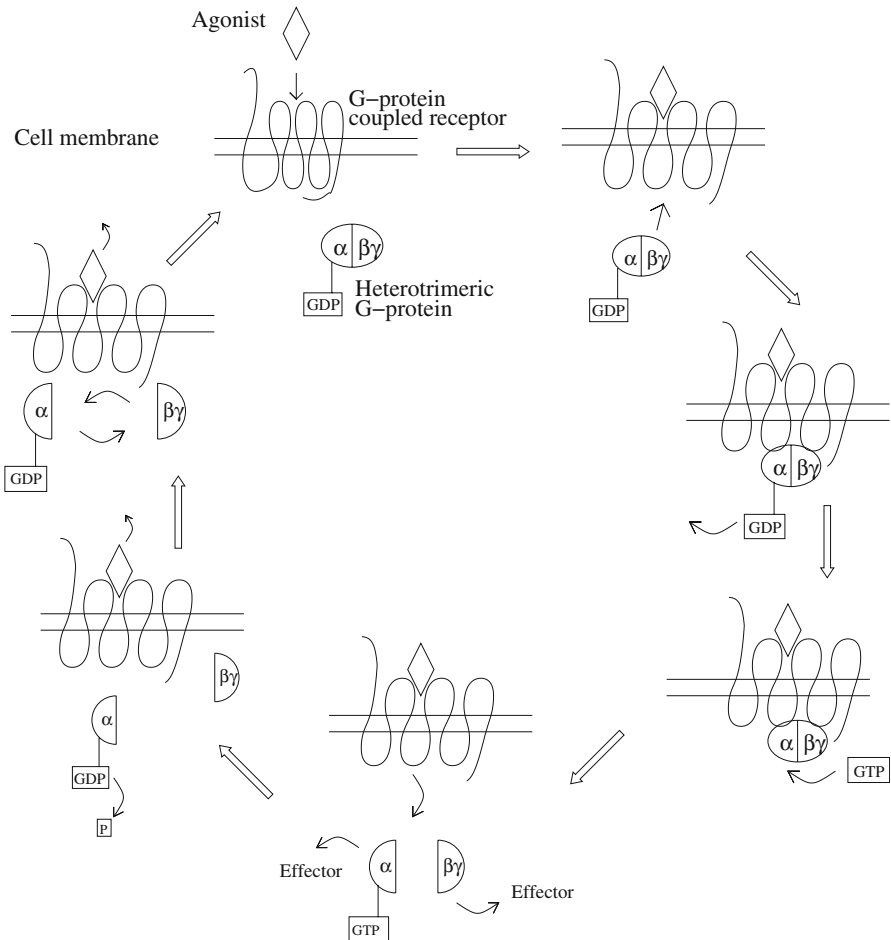
Fig. 3 G-protein activation (*right*)/deactivation (*left*) cycle: the shuttling mechanism

they are extremely susceptible to ligand binding, expressed below by the parameter ν. Upon ligand binding, the G-protein is activated (Lidow et al. 2001), as above.

A further complication is that receptors are not typically exclusive (i.e. they can be activated by more than one kind of ligand) and they can bind to more than one type of G-protein. It has been proposed that receptors may have more than one conformational state (Kenakin 1997; Leff et al. 1997). The basis of the theory is that the receptor has one inactive state, which is less willing to bind (i.e. has lower affinity), and multiple active states, each of which involves preferential binding to a different G-protein. To adopt some widely used terminology (Kenakin 1997), let R be the inactive receptor state of the β-adrenergic receptor, which is activated by adrenaline. Let R^* be the active form that binds to G_s-proteins and R^{**} the one that binds to G_i-proteins. The receptors can spontaneously change conformation between the three states and, in the absence of ligand, the receptors are distributed between the three states in equilibrium.

Constitutive receptor activity occurs when a noticeable response occurs in the absence of ligand. The most likely reason for this to happen is by receptor over-expression.

1.3 Previous work

There has been much experimental research conducted on GPCRs (see Alberts et al. 1994; Kenakin 1993, 1997; Watson and Arkinstall 1994, for example) which has led to the understanding outlined above. Only rather recently have attempts been made to model these systems mathematically, to test whether theoretical ideas about these processes can match up to experimental data.

De Lean et al. (1980) proposed one of the first models, the ternary complex model (TCM), in which both the G-protein and the ligand can interact with the receptor to form complexes. Nauroschat and an der Heiden (1996) extended this model by incorporating additional reactions to reflect second messenger production. Since then, receptors have been found to exist in differing conformations, the extended ternary complex model (eTCM) being formulated to reflect this discovery Kenakin (2001). Riccobene et al. (1999) and Adams et al. (1998) each used a variant of the eTCM and included desensitisation of the receptors. Woolf et al. (2001) used a variant of the eTCM with two different ligands to model membrane assays, which are used to measure the signal generated by a biological reporter. They also investigate the activated eTCM, which includes steps involving the activation of the G-protein by exchanging GDP for GTP and the dissociation of the α and $\beta\gamma$ subunits. It has been proposed that G-proteins can bind to inactive receptors: the relevant model is called the cubic ternary complex model (CTC), which is more thermodynamically complete than the TCM as it includes all the possible combinations of receptor and G-protein. Shea et al. (2000) introduced the activated CTC to study the dynamics of the G-protein activation process and were the first group to analyse any model dynamically. For a useful general review of all these models see Kenakin (2002).

Others have formulated similar models. Clément et al. (2001) considered the receptor/G-protein system as a single species which can be activated by a hormone. This active complex in turn activates adenylate cyclase to produce cAMP. Kukkonen et al. (2001) compare three models, namely: (1) the shuttling model, in which a ligand-activated receptor activates G-proteins, which freely diffuse away; (2) the complexing model, in which the activated G-protein remains bound to the receptor whilst interacting with the relevant enzyme; and (3) the pre-coupled model, in which the G-protein remains bound to the receptor even in the absence of ligand. Krakauer et al. (2002) also formulate an intracellular model utilising a G-protein pathway, where they (for mathematical simplicity) consider the G-protein to be part of a 'black box' mechanism in modelling the dynamics of the gonadotropic releasing hormone system. As noted above, receptors can bind to more than one type of G-protein; models with more than two active conformations have been formulated to reflect this, such as Chen et al. (2003) and Leff et al. (1997). Kinzer-Ursem and Linderman (2007) have recently investigated further the cubic ternary complex activation model.

The model we now outline is for a GPCR system which involves reactions with biological molecules that are present in sufficiently large numbers that deterministic

ordinary differential equation models should provide valuable insight. It is clearly desirable that detailed mathematical analysis be done on this system, as better understanding of the processes involved is necessary for efficient drug design and delivery.

1.4 Current work

In this paper, we present a model for drug-free G-protein activation that is thermodynamically sound, including reversible reactions in the G-protein cycle which have previously been treated as irreversible. We focus on constitutive receptor activity as a useful measure, and highlight the effects of various parameters on responses. Constitutive receptor activation is where the receptors alone, without the presence of ligand, can cause the G-proteins to become activated. This is done by over-expressing the receptor, i.e. by increasing the concentration of the receptor with respect to the concentration of the G-protein. Both the detailed background above, and the analysis which follows (which is designed to clarify the dynamics of the model via artificial initial data) is pursued in large part to provide a framework for investigating the much more important (and more complex) case of ligand binding. Further, the methods and analysis presented here are suggested as an approach for studying a number of further problems, including single ligand binding, competitive ligands binding, multiple receptor states and downstream signalling.

2 Model formulation

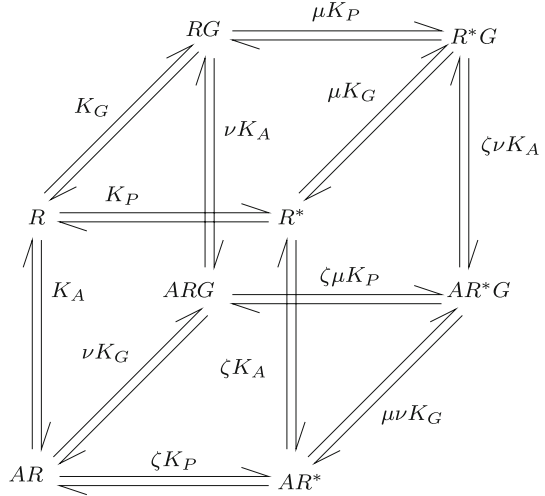### 2.1 Equilibrium considerations

2.1.1 Model assumptions

As our initial model, a receptor with one active state (R^*) and one inactive state (R) is chosen. All combinations of receptor (R or R^*), ligand (A) and G-protein (G) are allowed, other than the combination AG which is not included since the agonist cannot bind directly to the G-protein. This gives a total of eight different receptor states (see Fig. 4 for the eight states and the possible 'bimolecular' transitions between them). This model is called the cubic ternary complex model and, was analysed in equilibrium in Kenakin (2001). The model involves three equilibrium constants (K_A, K_G, K_P) and three thermodynamic constants (ζ, μ, ν). Rather than restrict our analysis to equilibrium states, in this paper, we present a study of the dynamics of G-protein activation, with no drug present. As such, we focus on the top face of the cube. A full discussion of the equilibrium and kinetic parameters appearing in the model is presented in Woodroffe et al. (2009); here, we include only those which do not involve ligand-bound receptors.

2.1.2 The equilibrium and thermodynamic constants

The equilibrium constants are defined as the ratio of the concentrations of the relevant species at equilibrium. K_G has units of M^{-1} and K_P is dimensionless. The relevant

Fig. 4 The eight basic receptor states

mass action expressions are

$$R + G \overset{K_G}{\rightleftharpoons} RG, \quad K_G = \frac{[RG]}{[R][G]}, \tag{1}$$

$$R \overset{K_P}{\rightleftharpoons} R^*, \quad K_P = \frac{[R^*]}{[R]}, \tag{2}$$

where here the [ ]'s denote equilibrium concentrations, with units of M.

The values of the thermodynamic constants characterise the role played by the different species involved in the equilibrium. The constant μ relates to the effects of the G-protein (rather than ligand) being bound; it appears, in particular, in the reactions

$$R + G \overset{K_G}{\rightleftharpoons} RG, \quad R^* + G \overset{\mu K_G}{\rightleftharpoons} R^*G, \tag{3}$$

$$R \overset{K_P}{\rightleftharpoons} R^*, \quad RG \overset{\mu K_P}{\rightleftharpoons} R^*G. \tag{4}$$

Increasing μ has the effect of making the G-proteins prefer to bind to R^* over R. It also sways the equilibrium of the receptor-G-protein complex towards R^*G.

We can relate the equilibrium concentrations of all the species, in terms of the thermodynamic constants, the equilibrium constants and the equilibrium concentrations of R, R^* and G, as follows

$$[RG] = K_G[R][G], \quad [R^*] = K_P[R], \tag{5}$$

$$[R^*G] = \mu K_G[R^*][G] = \mu K_P[RG] = \mu K_G K_P[R][G]. \tag{6}$$

These expressions encompass the various routes by which multi-step reactions can be achieved, which lead to a number of detailed balance constraints that relate the equilibrium constants. So far, only the interactions between the receptor and G-protein

have been addressed. In the next subsection, the activation of the receptor-G-protein complex will be considered.

2.2 Time dependent behaviour

2.2.1 Activation and deactivation rate constants

The active receptors bound to G-proteins (R^*G) are the ones that allow the exchange of the G-protein's GDP for GTP, thus activating it. The bound complexes can then dissociate into their $G_{\alpha-GTP}$ (henceforth to be denoted $\alpha^\dagger$), $G_{\beta\gamma}$ ($\beta\gamma$) and R^* components. Exchange and dissociation are taken to occur as a single step, with one rate constant k_{a+} [we note that exchange is expected to be slow compared to dissociation Shea et al. (2000)]. It will be assumed in this paper that this view of the dominant mechanism, known as the shuttling model, is biologically accurate. The complexing model, as considered by Kukkonen et al. (2001), whereby the α subunit remains bound to the receptor and thence forms a complex with the effector enzyme could be analysed in a similar fashion.

Rate constants are now introduced for all the reversible reactions, bearing in mind the relationships between the equilibrium constants given above, and also for the hydrolysis of the GTP on the $\alpha^\dagger$ back into GDP (by GTPase activity) and the recombination of $G_{\alpha-GDP}$ (α) and $\beta\gamma$. The relevant rate constants (shown in Fig. 5) are related to the equilibrium ones by

$$K_G = \frac{k_+}{k_-}, \quad K_P = \frac{k_p}{k_q}, \tag{7}$$

$$\zeta = \frac{\zeta_+}{\zeta_-}, \quad \mu = \frac{\mu_+}{\mu_-}, \quad v = \frac{v_+}{v_-}. \tag{8}$$

The constants can be identified by their subscripts, where

p the forward transition from R to R^*
q the reverse transition from R^* back to R
$+$ the process of binding the G-protein
$-$ the dissociation of the G-protein
$b+$ the reassociation of G from its inactive subunits
$g+$ the hydrolysis of $\alpha^\dagger$
$a+$ the activation of the G-protein complex and its dissociation into subunits

2.2.2 Parameter values

A literature survey has been conducted to find possible values for the constants in the model, Shea et al. (2000) and Riccobene et al. (1999) giving the most complete information, with Adams et al. (1998), Leff et al. (1997), Woolf et al. (2001) and Lemon et al. (2003) providing other values. To convert from (cell)$^{-1}$ to M^{-1} the value is multiplied by Avogadro's number (6.022×10^{23}) and divided by the number of cells

per litre [5×10^9 in the experimental set ups of Riccobene et al. (1999), Shea et al. (2000)]. A table of values is given in the Appendix.

2.2.3 Mathematical feasibility

The model includes rate constants which relate to the equilibrium constants in Eq. (7), and thermodynamic constants. It is necessary to break down the thermodynamic constants into forward and reverse components (denoted by $+$ or $-$) to reflect separately their influence on each of the forward and reverse reaction rates. The θ's indicate the possibility that the thermodynamic constant effects may be proportionately greater in different reactions.

The cubic ternary complex activation model (TCAM) includes three irreversible reactions, it being assumed in Shea et al. (2000) that $k_{b-} = k_{g-} = k_{a-} = 0$. While these assumptions may be reasonable, the reverse reactions are included here to give the model detailed balance. Figure 5 provides a schematic of all the relevant reactions. The system is not closed, since many reactions are governed by external processes, such as the hydrolysis of the GTP on the $\alpha^\dagger$ being governed by GTPase (which is generated by processes other than those in the model, included here within the value of k_{g+}), or the exchange of GTP and GDP since the GTP is formed elsewhere, implying in particular that the full system does not exhibit detailed balance, i.e. each individual reaction need not be in equilibrium when the entire system is.

We now define three more 'equilibrium' constants. For the reasons just noted, the associated equilibrium relations are not in fact satisfied at equilibrium, but they will be used in nondimensionalising the model. Indeed, since detailed balance of the system is negated by the move from the ternary complex model to the ternary complex activation model, the relations in Eqs. (1) and (2) do not hold at equilibrium either. These constants are

$$K_{act} = \frac{k_{a+}}{k_{a-}}, \quad K_{gtp} = \frac{k_{g+}}{k_{g-}}, \quad K_B = \frac{k_{b+}}{k_{b-}}, \tag{9}$$
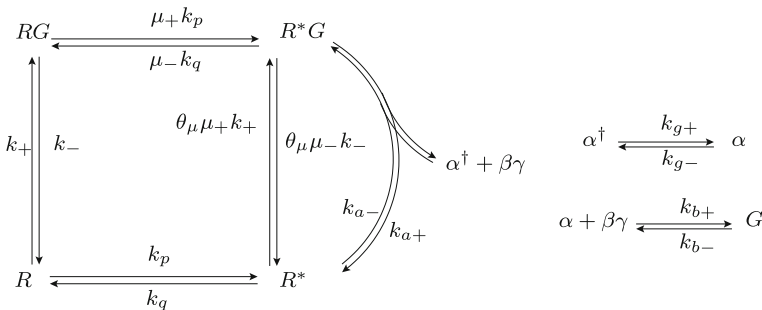

Fig. 5 The drug-free section of the cubic ternary complex activation model

and are derived from the relations

$$[R^*G] \overset{K_{act}}{\rightleftharpoons} [\alpha^\dagger] + [\beta\gamma] + [R], \quad [\alpha^\dagger] \overset{K_{gtp}}{\rightleftharpoons} [\alpha], \quad [\alpha] + [\beta\gamma] \overset{K_B}{\rightleftharpoons} [G]. \tag{10}$$

2.3 Dimensional differential equations

With the above assumptions and definitions, and using the law of mass action (as outlined in Murray (1993), for example) the model takes the form of a eighth-order system of ordinary differential equations as follows:

$$\frac{d[R]}{dt} = k_q[R^*] + k_-[RG] - (k_p + k_+[G])[R], \tag{11}$$

$$\frac{d[R^*]}{dt} = k_p[R] + \left(\mu_-\theta_\mu k_- + k_{a+}\right)[R^*G]$$
$$- (k_q + \theta_\mu\mu_+k_+[G] + k_{a-}[\alpha^\dagger][\beta\gamma])[R^*], \tag{12}$$

$$\frac{d[G]}{dt} = k_-[RG] + \theta_\mu\mu_-k_-[R^*G] + k_{b+}[\alpha][\beta\gamma]$$
$$- \left(k_+([R] + \theta_\mu\mu_+[R^*]) + k_{b-}\right)[G], \tag{13}$$

$$\frac{d[RG]}{dt} = k_+[R][G] + \mu_-k_q[R^*G] - (k_- + \mu_+k_p)[RG], \tag{14}$$

$$\frac{d[R^*G]}{dt} = \mu_+k_p[RG] + \theta_\mu\mu_+k_+[R^*][G] + k_{a-}[\alpha^\dagger][\beta\gamma][R^*]$$
$$- \left(\mu_-(k_q + \theta_\mu k_-) + k_{a+}\right)[R^*G], \tag{15}$$

$$\frac{d[\alpha]}{dt} = k_{g+}[\alpha^\dagger] + k_{b-}[G] - k_{b+}[\alpha][\beta\gamma] - k_{g-}[\alpha], \tag{16}$$

$$\frac{d[\alpha^\dagger]}{dt} = k_{a+}[R^*G] + k_{g-}[\alpha] - \left(k_{g+} + k_{a-}[R^*][\beta\gamma]\right)[\alpha^\dagger], \tag{17}$$

$$\frac{d[\beta\gamma]}{dt} = k_{a+}[R^*G] + k_{b-}[G] - k_{b+}[\alpha][\beta\gamma] - k_{a-}[R^*][\alpha^\dagger][\beta\gamma]. \tag{18}$$

Here $[\bullet]$ denotes the concentration of species $\bullet$. The quantities, R_{TOT}, the total number of receptors, and G_{TOT}, the total number of G-proteins are conserved. Moreover, the number of $\beta\gamma$ subunits is the same as the number of α and $\alpha^\dagger$ subunits, because each G splits into one α (or $\alpha^\dagger$) and one $\beta\gamma$, so if equality holds at $t = 0$ it does so for all t. Thus we have

$$R_{TOT} = [R] + [R^*] + [RG] + [R^*G], \tag{19}$$
$$G_{TOT} = [G] + [RG] + [R^*G] + [\alpha^\dagger] + [\alpha], \tag{20}$$
$$[\beta\gamma] = [\alpha^\dagger] + [\alpha], \tag{21}$$

with R_{TOT} and G_{TOT} constant.

The key differences between the current model and that of Shea et al. (2000) is that all the reactions here are reversible and the thermodynamic parameter set is complete.

This paper looks at the dynamics of the model in great detail, whereas Shea et al. (2000) only consider the time-course for a couple of cases, choosing instead to run the dynamic model to equilibrium in the majority of their study. The initial conditions adopted here are $R(0) = R_{TOT}$ and $G(0) = G_{TOT}$ with everything else set to zero, representing a sudden introduction of G-protein at $t = 0$, with negligible numbers of activated receptors being present initially. These initial conditions should allow us to investigate which reactions will be influential over which timescales. We now explore the dynamics of the model for these simple initial data.

3 Numerical solutions

3.1 Numerical method

The system has been studied numerically by two different methods in order to check consistency and accuracy. The first method uses a NAG routine (D02EJF), which implements a backward difference approach, and the second MATLAB's ode15s solver. The parameter values are those given in the Appendix. Figure 6a,b illustrate how R, G and α evolve to their equilibrium values; these will be used to rescale the variables in the next section, since approximate rescalings for the other species can be expressed in terms of these three using the equilibrium relations (5) and (6). As well as showing how the numerical equilibrium values were found, these figures indicate some interesting dynamical behaviour that will be investigated later.

With the parameter set in the Appendix the equilibrium values (denoted by a subscript e) in M are

$$R_e^* = 1.98 \times 10^{-13}, \qquad R_e = 1.98 \times 10^{-10}, \qquad G_e = 1.52 \times 10^{-10}, \qquad (22)$$

$$RG_e = 2.12 \times 10^{-10}, \qquad R^*G_e = 4.33 \times 10^{-13}, \qquad \alpha_e = 4.1 \times 10^{-11}, \qquad (23)$$

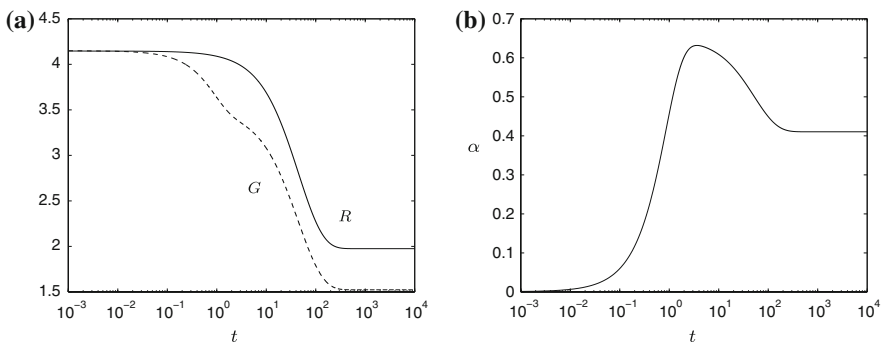$$\alpha_e^\dagger = 4.4 \times 10^{-12}, \qquad \beta\gamma_e = 4.5 \times 10^{-11}. \qquad (24)$$

Fig. 6 Numerical results for **a** R, G and **b** α. Note that here, and in subsequent dimensional plots, the concentration of the species has been rescaled for viewing convenience from $O(10^{-10})$ to $O(1)$ by multiplying by 10^{10}
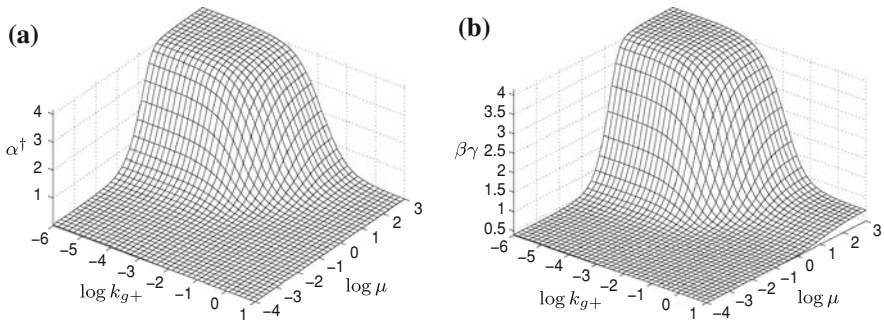
(a)

(b)

Fig. 7 Equilibrium values of **a** $\alpha^\dagger$, and **b** $\beta\gamma$ against μ and k_{g+}, the other parameter values here and henceforth being those given in the Appendix

3.2 GTPase action and receptor activation

Here we modify the value of μ to model the effect of the receptor being more or less keen to become activated when bound to a G-protein. We also change the value of k_{g+}, representing an increase in GTPase activity, mimicking the effect of GAP proteins, the action of GTPase (and GAP proteins) being to convert $\alpha^\dagger$ back to α. Results are shown in Fig. 7a, with the output $\alpha^\dagger$ increasing with μ to an upper limit. This follows intuition, as increasing μ should increase the propensity of RG to become activated, forming R^*G and thus increasing the concentration $\alpha^\dagger$. Hence we can say that, at least for sufficiently small GTPase action, increasing μ enhances constitutive receptor activation. The dependence on k_{g+} is equally unsurprising: when k_{g+} is increased, representing an increase of GTPase action, the response in $\alpha^\dagger$ decreases to zero.

Figure 7b demonstrates similar behaviour for $\beta\gamma$, though its lowest value is not zero (as for $\alpha^\dagger$), but about 5×10^{-11}M. This is because the $\beta\gamma$ is formed from either the dissociation of the G-protein or from the dissociation of R^*G, the former being independent of μ or k_{g+}. It can be seen that as μ increases, the proportion of free $\beta\gamma$ increases, since not so much of it is contained in the dominant RG complex. Increasing GTPase action (i.e. k_{g+}) has the expected effect of reducing $\beta\gamma$, since the latter binds more rapidly to α to reform the G-protein.

3.3 Receptor overexpression

Now we change the total number of receptors and G-proteins to model constitutive receptor activity. Figure 8 illustrates how the response changes with increasing R_{TOT}.

If the total concentration of receptors is similar to the total concentration of G-protein ($\log_{10}(R_{TOT}/G_{TOT}) \approx 1$), then we see a basal level of response of about $\alpha^\dagger = 4 \times 10^{-12}$M. Increasing the relative concentration of R_{TOT} tenfold increases the response by a factor of approximately two. If the G-protein is usually present in amounts corresponding to approximately ten times that of receptor, as some literature suggests (Woolf et al. 2001), then the response is significantly lower and a (possibly biologically unfeasible) hundredfold increase in receptor concentration from that
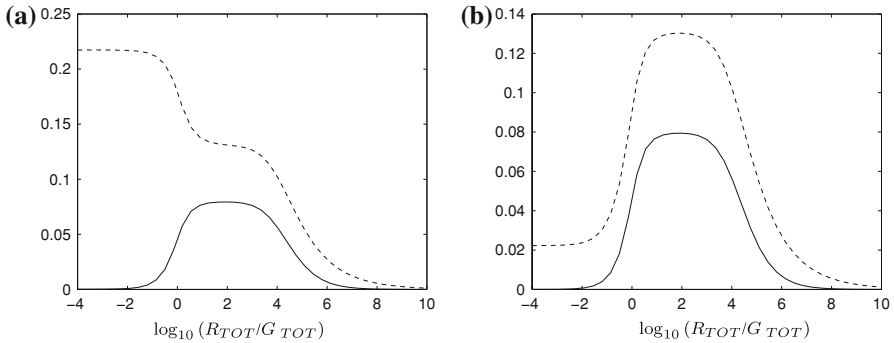
Fig. 8 Graph for $[\alpha^{\dagger}]$ (*solid*) and $[\beta\gamma]$ (*dashed*) plotted against $\log_{10}(R_{TOT}/G_{TOT})$ with constant $G_{TOT} = 4.15 \times 10^{-10}$ M to demonstrate constitutive receptor activation for **a** $k_{b-} = 0.0144$; **b** $k_{b-} = 0.000144$
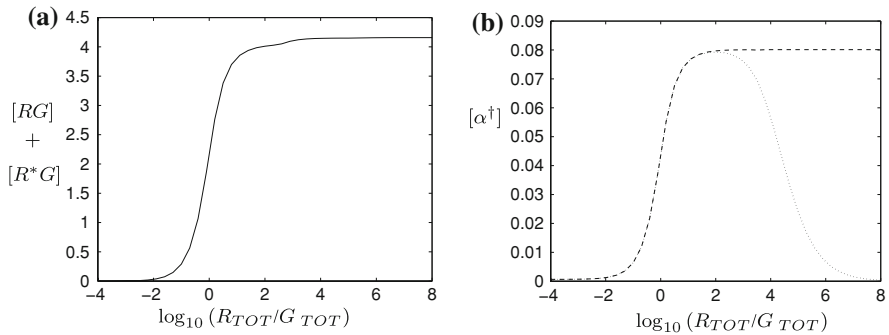

Fig. 9 Graphs with **a** $[RG]$ plotted against $\log_{10}(R_{TOT}/G_{TOT})$ with constant $G_{TOT} = 4.15 \times 10^{-10}$ M to demonstrate the reversal of constitutive receptor activation as R_{TOT} gets large; **b** $[\alpha^{\dagger}]$ plotted against $\log_{10}(R_{TOT}/G_{TOT})$ for $k_{a-} = 10^{18}$ M^{-2}s^{-1} (*dotted*) and $k_{a-} = 0$ (*dashed*) to show the reverse activation reaction causes signal killing at high receptor levels

level would be required to increase the response by a factor of approximately ten. This receptor overexpression clearly demonstrates constitutive receptor activity. It can be seen from the model (particularly, the first term in the right hand side of Eq. (14)) that as the concentration of receptor increases, more G-protein can become bound, and so more can become activated and dissociate from the receptors. How this constitutive activity is affected by inverse agonists is of particular interest, and this is explored in Woodroffe et al. (2009).

A surprise comes at even higher concentrations of receptor, namely where the concentration is approximately 10^4 times that of the G-protein. This may not be a physiologically realistic situation, but it is interesting mathematically. When the level of receptors gets very large, so many are available to bind to the G-proteins that the latter in effect become trapped in complexes, i.e. as soon as they become activated and dissociate, they are snapped up again by another receptor. This can be seen in Fig. 9a, where the concentration of RG tends to G_{TOT}. In fact, this result can be explained by looking at the reaction

$$[R^*G] \underset{k_{a-}}{\overset{k_{a+}}{\rightleftharpoons}} [R^*] + [\alpha^\dagger] + [\beta\gamma], \tag{25}$$

wherein k_{a-} is small in view of the 'near-irreversibility' of the reaction. Usually, its effect is negligible, with the majority of the $\alpha^\dagger$ being converted to α through GTPase action with a very small amount combining with $\beta\gamma$ and R^* to reform R^*G. However, if the concentration of receptor rises to a very high level, the reverse step in the above reaction can become dominant, with any free $\alpha^\dagger$ quickly bound to receptor. This is demonstrated in Fig. 9b, where the dashed line corresponding to $k_{a-} = 0$ exhibits a plateau. This illustrates how violating detailed balance in the system of equations by assuming some reactions to be irreversible leads to erroneous qualitative behaviour. While there appears to be little difference for $\log_{10}(R_{TOT}/G_{TOT}) < 1$, which corresponds to experimental data summarised in Table 1, taking $k_{a-} = 0$ is not sufficient to capture the mopping-up effect of high receptor concentration.

It is instructive to note that constitutive receptor activity is not exhibited by the $\beta\gamma$ subunits for $k_{b-} > 0.005$ (Fig. 8a); for these values, the maximal free $\beta\gamma$ response comes at negligible receptor numbers. In the absence of receptor, approximately 7% of the G-protein is dissociated due to the relatively high value of k_{b-}. As R_{TOT} increases to become comparable to G_{TOT}, the $\beta\gamma$ concentration ($\beta\gamma$ response) starts decreasing as the available G-protein gets taken up by the receptors, decreasing the proportion dissociated. Then, as the increase in receptor concentration produces a greater $\alpha^\dagger$ response, a plateau is seen in the regime of greatest $\alpha^\dagger$ response; the second effect then comes in to play at about $R_{TOT}/G_{TOT} = 10^4$ when the receptors aggressively take up the G-proteins. For lower values of k_{b-}, constitutive receptor activation can be seen in $[\beta\gamma]$ (Fig. 8b) as, without receptor, only about 0.023×10^{-10}M (0.5% of the total G-protein) is dissociated. In Fig. 10, we show the effect of receptor overexpression on $\alpha^\dagger$ and $\beta\gamma$ responses over a range of values of k_{b-}. Increasing receptor concentration leads to an increased $\alpha^\dagger$ response for all k_{b-}, up to a maximum occurring when $R_{TOT}/G_{TOT} \approx 100$. In Fig. 10c , we clearly see that for $k_{b-} < 0.005$, the maximal $\beta\gamma$ response occurs at the same receptor level.
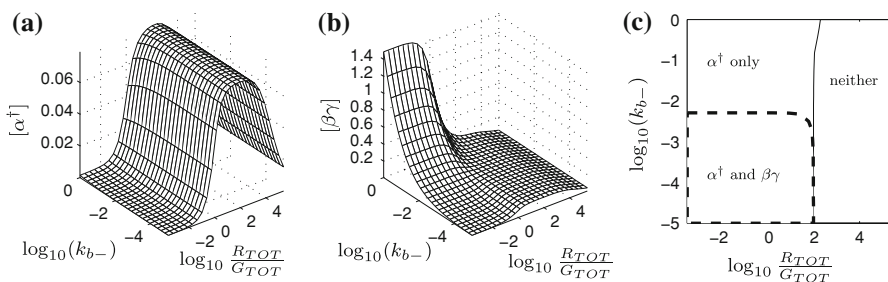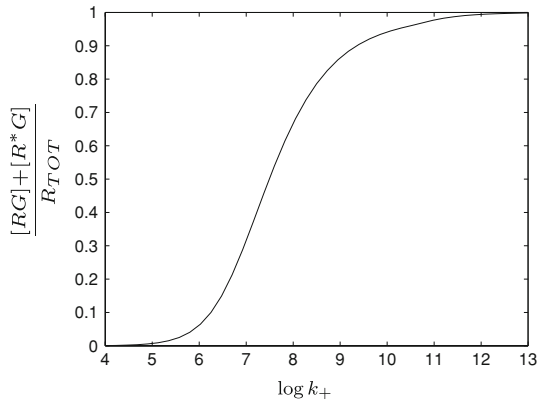

Fig. 10 Constitutive receptor activity demonstrated in $\alpha^\dagger$ and $\beta\gamma$ responses. **a** $\alpha^\dagger$ response; **b** $\beta\gamma$ response; **c** regions of (R_{TOT}, k_{b-}) space where receptor overexpression leads to increased response for $\alpha^\dagger$ only, both $\alpha^\dagger$ and $\beta\gamma$, and neither $\alpha^\dagger$ nor $\beta\gamma$

Fig. 11 Graph to show how precoupling of receptors and G-protein increases with k_+

3.4 Pre-coupling

In this section we investigate how the equilibrium constant K_G affects the pre-coupling of receptors and G-proteins in the absence of drug. The result is shown in Fig. 11. It is not surprising that as k_+ increases (and, hence, K_G increases) the proportion of precoupled receptor increases; the result does, however, have significant implications when ligand is included, as we shall discuss elsewhere.

4 Asymptotic analysis

4.1 Non-dimensionalisation

4.1.1 Rescaling

To non-dimensionalise the system of Eqs. (11)–(18), we rescale with the equilibrium values for R, G, and α derived numerically in Eqs. (22) and (24) and with the other equilibrium values satisfying the relations

$$K_{act} = \frac{[\alpha^\dagger][\beta\gamma][R^*]}{[R^*G]}, \quad K_{gtp} = \frac{[\alpha]}{[\alpha^\dagger]}, \quad K_B = \frac{[G]}{[\alpha][\beta\gamma]}, \tag{26}$$

and Eqs. (5) and (6). We thus set

$$r = \frac{[R]}{R_e}, \qquad r^* = \frac{[R^*]}{R_e K_P}, \quad g = \frac{[G]}{G_e}, \qquad p = \frac{[RG]}{K_G R_e G_e}, \tag{27}$$

$$p^* = \frac{[R^*G]}{\mu K_G K_P R_e G_e}, \quad x = \frac{[\alpha]}{\alpha_e}, \qquad x^\dagger = \frac{K_{gtp}[\alpha^\dagger]}{\alpha_e}, \quad z = \frac{K_B \alpha_e[\beta\gamma]}{G_e}. \tag{28}$$

This notation was adopted because r corresponds to receptor, p to *pre*-coupled receptor; x and z represent α and $\beta\gamma$ respectively. The *’s represents activation and the

† represents GTP binding. We note that other scalings may be used, but those chosen here are sensible, given that we have already found the equilibrium values numerically.

4.1.2 Non-dimensional differential equations

To form a system of non-dimensional ordinary differential equations, we introduce $\tilde{t} = k_q t$, i.e. we scale time on the basis of the reaction $R \rightleftharpoons R^*$, which we anticipate will be one of the fastest, giving the system

$$\frac{dr}{d\tilde{t}} = K_P(r^* - r) + \tilde{k}_+(p - rg) \tag{29}$$

$$\frac{dr^*}{d\tilde{t}} = r - r^* + \theta_\mu \mu_+ \tilde{k}_+(p^* - gr^*) + \frac{\tilde{k}_+}{\tilde{k}_-}(\mu \tilde{k}_{a+} p^* - \tilde{k}_{a-} r^* x^\dagger z), \tag{30}$$

$$\frac{dg}{d\tilde{t}} = \rho_1 \tilde{k}_+ \left(p - gr + \mu_+ K_P(p^* - gr^*) \right) + \frac{\rho_1}{\rho_2} \tilde{k}_{b-}(xz - g), \tag{31}$$

$$\frac{dp}{d\tilde{t}} = \tilde{k}_-(gr - p) + \mu_+ K_P(p^* - p), \tag{32}$$

$$\frac{dp^*}{d\tilde{t}} = \mu_-(p - p^*) + \theta_\mu \mu_- \tilde{k}_-(gr^* - p^*) + \frac{\tilde{k}_{a-}}{\mu} r^* x^\dagger z - \tilde{k}_{a+} p^*, \tag{33}$$

$$\frac{dx}{d\tilde{t}} = \tilde{k}_{g-}(x^\dagger - x) + \tilde{k}_{b-}(g - xz), \tag{34}$$

$$\frac{dx^\dagger}{d\tilde{t}} = \rho_2 K_P \frac{\tilde{k}_+ \tilde{k}_{g+}}{\tilde{k}_- \tilde{k}_{g-}} \left(\mu \tilde{k}_{a+} p^* - \tilde{k}_{a-} r^* x^\dagger z \right) + \tilde{k}_{g+}(x - x^\dagger), \tag{35}$$

$$\frac{dz}{d\tilde{t}} = \rho_2 K_P \frac{\tilde{k}_{b+} \tilde{k}_+}{\tilde{k}_{b-} \tilde{k}_-} \left(\mu \tilde{k}_{a+} p^* - \tilde{k}_{a-} r^* x^\dagger z \right) + \tilde{k}_{b+}(g - xz), \tag{36}$$

where the fourteen independent non-dimensionalised parameters are

$$\tilde{k}_+ = \frac{k_+ G_e}{k_q}, \qquad \tilde{k}_- = \frac{k_-}{k_q}, \qquad \tilde{k}_{g+} = \frac{k_{g+}}{k_q}, \qquad \tilde{k}_{g-} = \frac{k_{g-}}{k_q},$$

$$\tilde{k}_{a+} = \frac{k_{a+}}{k_q}, \qquad \tilde{k}_{a-} = \frac{k_{a-}}{k_q K_B K_{gtp} K_G}, \qquad \tilde{k}_{b+} = \frac{k_{b+} \alpha_e}{k_q}, \qquad \tilde{k}_{b-} = \frac{k_{b-} G_e}{\alpha_e k_q},$$

$$K_P = \frac{k_p}{k_q}, \qquad \mu_+, \qquad \mu_-, \qquad \theta_\mu,$$

$$\rho_1 = R_e/G_e, \qquad \rho_2 = R_e/\alpha_e, \tag{37}$$

with one dependent parameter, $\mu = \mu_+/\mu_-$. The initial conditions are

$$r(0) = \frac{R_{TOT}}{R_e} = r_e, \quad g(0) = \frac{G_{TOT}}{G_e} = g_e, \tag{38}$$

with all the other variables equal to zero.

Fig. 12 Numerics for r^* and x to indicate the three distinct timescales. Note the logarithmic scale for time
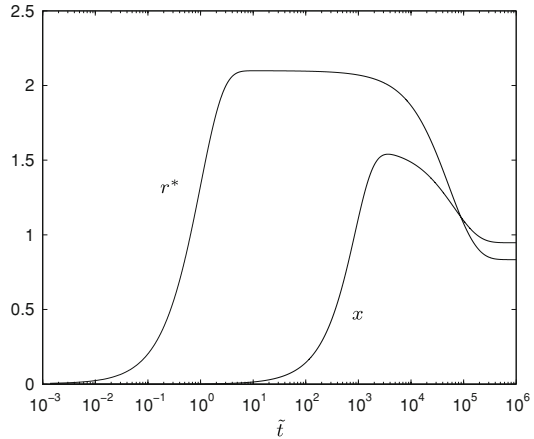
4.2 Timescale considerations

Figure 12 demonstrates the existence of widely different timescales. Now analyses will be carried out on the system to attempt to understand better the numerical results. As the system is too complicated to solve exactly, asymptotic approximations will be made over the various timescales.

To analyse the system, the parameters need to be rescaled by their approximate values, in terms of K_P (which seems to in practice to be a key small quantity). The physiological meaning of $K_P \ll 1$ is that $[R] \gg [R^*]$ in equilibrium; on the basis of the parameter values in the Appendix, we set

$$K_P = 10^{-3} = \epsilon, \qquad\qquad \tilde{k}_+ = 5.48 \times 10^{-6} = \lambda_+ \epsilon^2, \qquad (39)$$

$$\tilde{k}_- = 3 \times 10^{-6} = \lambda_- \epsilon^2, \qquad\qquad \rho_1 = 1.3 = O(1), \qquad (40)$$

$$\tilde{k}_{b-} = 0.534 \times 10^{-3} = \lambda_{b-}\epsilon, \qquad \tilde{k}_{a+} = 10^{-3} = \lambda_{a+}\epsilon, \qquad (41)$$

$$\rho_2 = 4.81 = O(1), \qquad\qquad \tilde{k}_{b+} = 0.495 \times 10^{-3} = \lambda_{b+}\epsilon, \qquad (42)$$

$$\tilde{k}_{g-} = 10^{-7} = \lambda_{g-}\epsilon^{5/2}, \qquad\qquad \mu_+ = 1 = O(1), \qquad (43)$$

$$\tilde{k}_{a-} = 10^{-9} = \lambda_{a-}\epsilon^3, \qquad\qquad \tilde{k}_{g+} = 10^{-4} = \lambda_{g+}\epsilon^{3/2}, \qquad (44)$$

$$\theta_\mu = 1 = O(1), \qquad\qquad \mu_- = 0.5 = O(1). \qquad (45)$$

All the resulting parameters other than ϵ will thus be treated as $O(1)$. There is of course some ambiguity in the choices of scalings with respect to ϵ but, since we shall focus for the most part on the leading order problems on each timescale, this is in fact of little significance.

An asymptotic approach is now used to analyse the nonlinear model. This method is here useful for several reasons: in particular, the expansion in a small parameter makes the reduced systems analytically tractable, with sufficient terms to give excellent quantitative accuracy readily being obtained; moreover, the approach sheds light on the reaction steps which control the evolution over each of the disparate timescales.

We note that we follow common practice in determining each timescale from the disordering of the expansion of the previous one.

4.3 Short-time asymptotics: $t = O(1)$

The timescale $t = O(1)$ typically corresponds in dimensional terms to times of order 10^{-3} s. The system of ordinary differential equations is then, dropping tildes,

$$\frac{dr}{dt} = \epsilon(r^* - r) + \lambda_+ \epsilon^2(p - gr), \tag{46}$$

$$\frac{dr^*}{dt} = r - r^* + \theta_\mu \mu_+ \lambda_+ \epsilon^2(p^* - gr^*) + \frac{\lambda_+}{\lambda_-}\epsilon(\mu\lambda_{a+}p^* - \epsilon^2\lambda_{a-}r^*x^\dagger z), \tag{47}$$

$$\frac{dg}{dt} = \rho_1\lambda_+ \epsilon^2(p - gr + \mu_+\epsilon(p^* - gr^*)) + \frac{\rho_1}{\rho_2}\lambda_{b-}\epsilon(xz - g), \tag{48}$$

$$\frac{dp}{dt} = \lambda_- \epsilon^2(gr - p) + \mu_+\epsilon(p^* - p), \tag{49}$$

$$\frac{dp^*}{dt} = \mu_-(p - p^*) + \theta_\mu \mu_- \lambda_- \epsilon^2(gr^* - p^*) + \frac{\lambda_{a-}}{\mu}\epsilon^3 r^*x^\dagger z - \lambda_{a+}\epsilon p^*, \tag{50}$$

$$\frac{dx}{dt} = \lambda_g \epsilon^{5/2}(x^\dagger - x) + \lambda_b \epsilon(g - xz), \tag{51}$$

$$\frac{dx^\dagger}{dt} = \rho_2\epsilon\frac{\lambda_g + \lambda_+}{\lambda_g - \lambda_-}(\mu\lambda_{a+}p^* - \lambda_{a-}\epsilon^2 r^*x^\dagger z) + \lambda_{g+}\epsilon^{3/2}(x - x^\dagger), \tag{52}$$

$$\frac{dz}{dt} = \rho_2\epsilon^2\frac{\lambda_b + \lambda_+}{\lambda_b - \lambda_-}(\mu\lambda_{a+}p^* - \lambda_{a-}\epsilon^2 r^*x^\dagger z) + \lambda_{b+}\epsilon(g - xz). \tag{53}$$

It can be seen from the initial conditions (38) that r and g will be $O(1)$ on this timescale and in consequence so will r^*. From the sizes of the terms in (51), (53) we see that $x, z = O(\epsilon)$ and so on, the full set of appropriate scalings being

$$p = \epsilon^2\tilde{p}, \qquad p^* = \epsilon^2\tilde{p}^*, \qquad x = \epsilon\tilde{x}, \qquad x^\dagger = \epsilon^{5/2}\tilde{x}^\dagger, \tag{54}$$

$$z = \epsilon\tilde{z}, \qquad r = \tilde{r}, \qquad r^* = \tilde{r}^*, \qquad g = \tilde{g}. \tag{55}$$

These imply that

$$\frac{d\tilde{r}}{dt} = \epsilon(\tilde{r}^* - \tilde{r}) + \lambda_+ \epsilon^2(\epsilon^2\tilde{p} - \tilde{g}\tilde{r}), \tag{56}$$

$$\frac{d\tilde{r}^*}{dt} = \tilde{r} - \tilde{r}^* + \theta_\mu \mu_+ \lambda_+ \epsilon^2(\epsilon^2\tilde{p}^* - \tilde{g}\tilde{r}^*) + \frac{\lambda_+}{\lambda_-}\epsilon^3(\mu\lambda_{a+}\tilde{p}^* - \lambda_{a-}\epsilon^{7/2}\tilde{r}^*\tilde{x}^\dagger\tilde{z}), \tag{57}$$

$$\frac{d\tilde{g}}{dt} = \rho_1\lambda_+ \epsilon^2(\epsilon^2\tilde{p} - \tilde{g}\tilde{r} + \mu_+\epsilon(\epsilon^2\tilde{p}^* - \tilde{g}\tilde{r}^*)) + \frac{\rho_1}{\rho_2}\lambda_{b-}\epsilon(\epsilon^2\tilde{x}\tilde{z} - \tilde{g}), \tag{58}$$

$$\frac{d\tilde{p}}{dt} = \lambda_-(\tilde{g}\tilde{r} - \epsilon^2\tilde{p}) + \mu_+\epsilon(\tilde{p}^* - \tilde{p}), \tag{59}$$

$$\frac{d\tilde{p}^*}{dt} = \mu_-(\tilde{p} - \tilde{p}^*) + \theta_\mu \mu_- \lambda_-(\tilde{g}\tilde{r}^* - \epsilon^2 \tilde{p}^*) + \frac{\lambda_{a-}}{\mu} \epsilon^{9/2} \tilde{r}^* \tilde{x}^\dagger \tilde{z} - \lambda_{a+} \epsilon \tilde{p}^*, \quad (60)$$

$$\frac{d\tilde{x}}{dt} = \lambda_{g-} \epsilon^{5/2}(\epsilon \tilde{x}^\dagger - \tilde{x}) + \lambda_{b-}(\tilde{g} - \epsilon^2 \tilde{x}\tilde{z}), \quad (61)$$

$$\frac{d\tilde{x}^\dagger}{dt} = \rho_2 \epsilon^{1/2} \frac{\lambda_{g+}\lambda_+}{\lambda_{g-}\lambda_-}(\mu\lambda_{a+}\tilde{p}^* - \lambda_{a-}\epsilon^{7/2}\tilde{r}^*\tilde{x}^\dagger\tilde{z}) + \lambda_{g+}(\tilde{x} - \epsilon^{3/2}\tilde{x}^\dagger), \quad (62)$$

$$\frac{d\tilde{z}}{dt} = \rho_2 \epsilon^3 \frac{\lambda_{b+}\lambda_+}{\lambda_{b-}\lambda_-}(\mu\lambda_{a+}\tilde{p}^* - \lambda_{a-}\epsilon^{7/2}\tilde{r}^*\tilde{x}^\dagger\tilde{z}) + \lambda_{b+}(\tilde{g} - \epsilon^2 \tilde{x}\tilde{z}). \quad (63)$$

Substituting

$$\tilde{r} = \tilde{r}_0 + \epsilon^{1/2}\tilde{r}_1 + \epsilon\tilde{r}_2 + \cdots, \quad (64)$$

etc. into (56)–(63) gives us the leading order equations

$$\frac{d\tilde{r}_0}{dt} = 0, \quad \frac{d\tilde{r}_0^*}{dt} = \tilde{r}_0 - \tilde{r}_0^*, \quad \frac{d\tilde{p}_0}{dt} = \lambda_- \tilde{g}_0 \tilde{r}_0, \quad \frac{d\tilde{p}_0^*}{dt} = \mu_-(\tilde{p}_0 - \tilde{p}_0^* + \theta_\mu \lambda_- \tilde{g}_0 \tilde{r}_0^*), \quad (65)$$

$$\frac{d\tilde{g}_0}{dt} = 0, \quad \frac{d\tilde{x}_0}{dt} = \lambda_{b-} \tilde{g}_0, \quad \frac{d\tilde{x}_0^\dagger}{dt} = \lambda_{g+} \tilde{x}_0, \quad \frac{d\tilde{z}_0}{dt} = \lambda_{b+} \tilde{g}_0, \quad (66)$$

having explicit leading order solutions

$$\tilde{r}_0 = r_e, \qquad \tilde{r}_0^* = r_e(1 - e^{-t}), \qquad \tilde{x}_0^\dagger = \frac{1}{2}\lambda_{g+}\lambda_{b-}g_e t^2, \quad (67)$$

$$\tilde{p}_0 = \lambda_- r_e g_e t, \qquad \tilde{x}_0 = \lambda_{b-} g_e t, \qquad \tilde{z}_0 = \lambda_{b+} g_e t, \quad (68)$$

$$\tilde{p}_0^* = \lambda_- r_e g_e \left(\theta_\mu - \frac{1}{\mu_-} + t + \frac{\theta_\mu \mu_-}{1 - \mu_-}e^{-t} + \left(\frac{1}{\mu_-} - \frac{\theta_\mu}{1 - \mu_-}\right)e^{-\mu_- t}\right), \quad \tilde{g}_0 = g_e. \quad (69)$$

We find that $\tilde{r}_1 = \tilde{r}_1^* = \tilde{g}_1 = \tilde{x}_1 = \tilde{z}_1 = \tilde{r}_3 = \tilde{r}_3^* = \tilde{g}_3 = 0$ and construct non-trivial correction terms in the form

$$\tilde{r}_2 = r_e(e^{-t} - 1), \qquad \tilde{r}_4 = r_e(-te^{-t} - e^{-t} - \lambda_+ g_e t + 1), \quad (70)$$

$$\tilde{r}_2^* = r_e(te^{-t} + e^{-t} - 1), \quad \tilde{r}_4^* = r_e\left(1 - \left(1 - t + \frac{t^2}{2}\right)e^{-t} + \lambda_+ g_e t\left(e^{-t} - 1\right)\right), \quad (71)$$

$$\tilde{g}_2 = -\frac{\rho_1}{\rho_2}\lambda_{b-}g_e t, \qquad \tilde{g}_4 = -\rho_1 \lambda_+ r_e g_e t + \frac{\rho_1^2}{\rho_2^2}\lambda_{b-}^2 g_e \frac{t^2}{2}, \quad (72)$$

$$\tilde{x}_2 = -\frac{\rho_1}{\rho_2}\lambda_{b-}^2 g_e \frac{t^2}{2}, \qquad \tilde{z}_2 = -\frac{\rho_1}{\rho_2}\lambda_{b-}\lambda_{b+}g_e \frac{t^2}{2}. \quad (73)$$

By comparing $\tilde{x}_0$ and $\tilde{x}_2$, say, it can be seen that at $t = O(\epsilon^{-1})$, the expansion disorders. The reactions operating on this fast timescale to leading order are $R \rightleftharpoons R^*$,
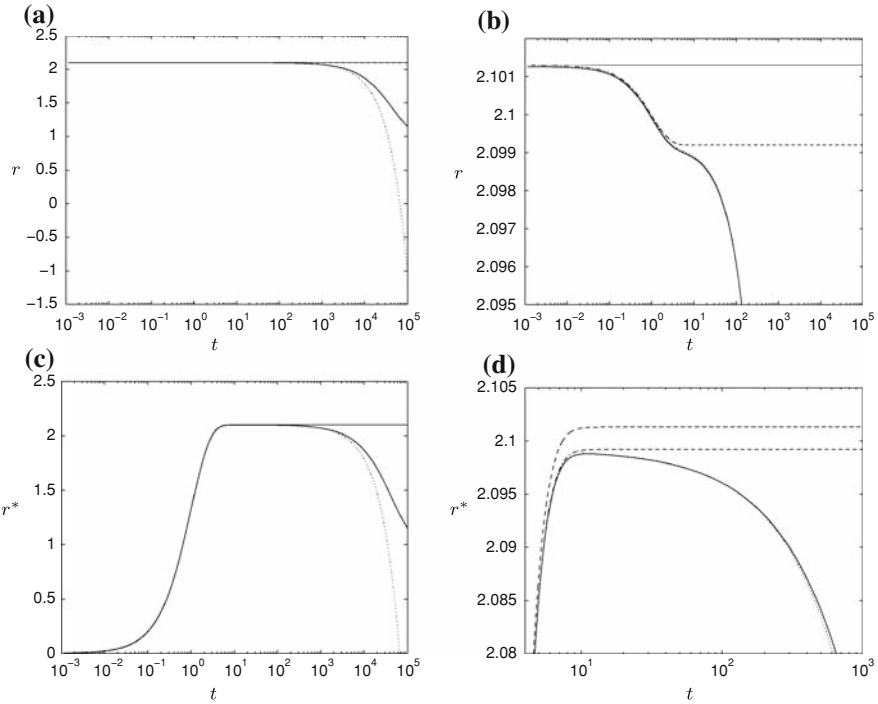
(a)

(b)

(c)

(d)

Fig. 13 Numerics (*solid line*) and short-time asymptotics. '$---$' represents the leading-order solutions, '$-\cdot-$' solutions up to $O(\epsilon)$, '$\cdots\cdots$' solutions up to $O(\epsilon^2)$. **a** r; **b** close-up of **a**; **c** r^*; **d** close-up of **c**
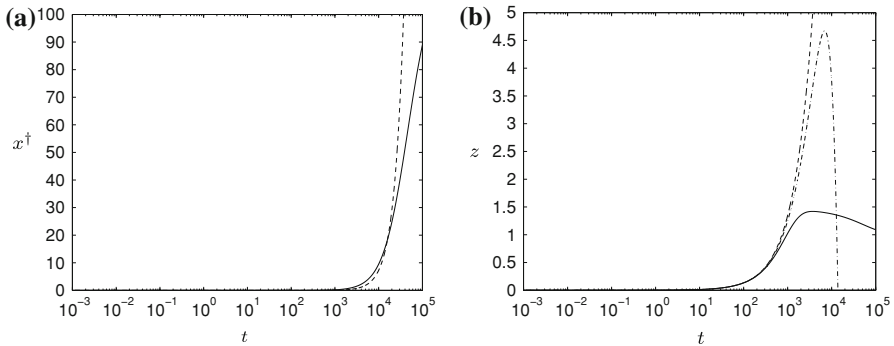
(a)

(b)

Fig. 14 Numerics (*solid line*) and short-time asymptotics. '$---$' represents the leading-order solutions, '$-\cdot-$' in (b) solutions up to $O(\epsilon)$. **a** $x^\dagger$; **b** z

$RG \rightleftharpoons R^*G$, $G \rightarrow \alpha + \beta\gamma$, $R + G \rightarrow RG$, $\alpha \rightarrow \alpha^\dagger$ and $R^* + G \rightarrow R^*G$. The reaction $R \rightleftharpoons R^*$ remains in equilibrium throughout all the following timescales. The kink seen in r in Fig. 13b comes from the very fast conformational change, converting r into r^*. As can be seen in Figs. 13, 14 and 15, the analysis only works for sufficiently small times $\tilde{t} \ll \epsilon^{-1}$, consistent with the remarks above. We have seen that the behaviour at this timescale is largely governed by the reaction $R \rightleftharpoons R^*$, this and
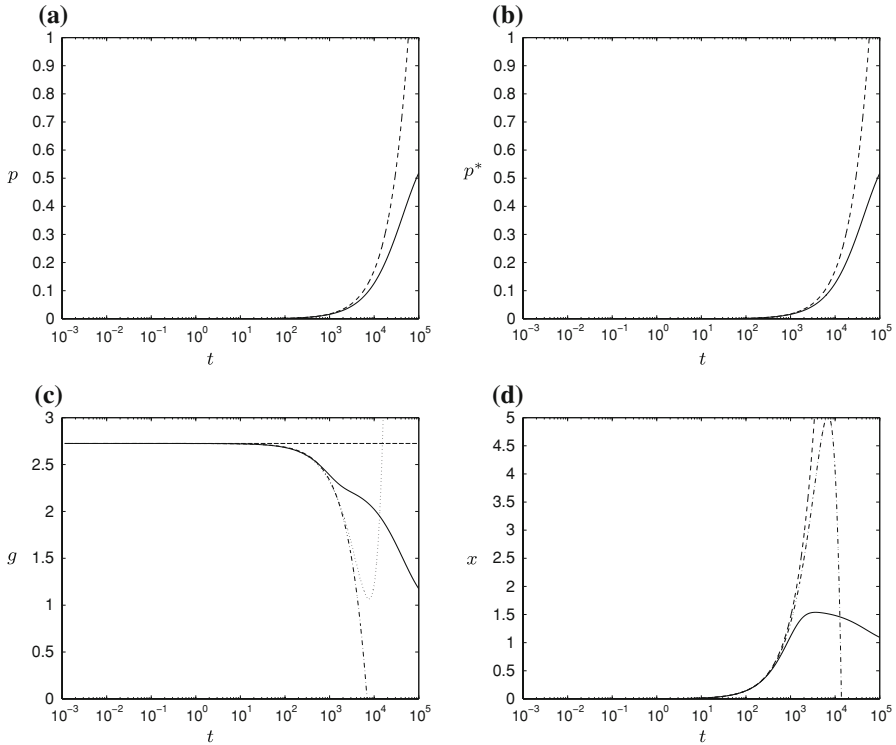
Fig. 15 Numerics (*solid line*) and short-time asymptotics. '– – –' represents the leading-order solutions, '– · –·' solutions up to $O(\epsilon)$, '······' solutions up to $O(\epsilon^2)$. **a** p; **b** p^*; **c** g; **d** x

$RG \rightleftharpoons R^*G$ being the only reactions that come to equilibrium. The asymptotics for x and z do not appear to follow the numerics closely for very long. However, within the timescale involved they match closely with the numerics.

4.4 Intermediate-time asymptotics: $t = O(\epsilon^{-1})$

Setting $T = \epsilon t$ in Eqs. (46)–(53), and (in view of (67)–(73)) $p = \epsilon \hat{p}$, $p^* = \epsilon \hat{p}^*$, $x^\dagger = \epsilon^{1/2} \hat{x}^\dagger$, $r = \hat{r}$, $r^* = \hat{r}^*$, $g = \hat{g}$, $x = \hat{x}$ and $z = \hat{z}$ gives

$$\frac{d\hat{r}}{dT} = \hat{r}^* - \hat{r} + \lambda_+ \epsilon (\epsilon \hat{p} - \hat{g}\hat{r}), \tag{74}$$

$$\epsilon \frac{d\hat{r}^*}{dT} = \hat{r} - \hat{r}^* + \theta_\mu \mu_+ \lambda_+ \epsilon^2 (\epsilon \hat{p}^* - \hat{g}\hat{r}^*) + \frac{\lambda_+}{\lambda_-} \epsilon^2 (\mu \lambda_{a+} \hat{p}^* - \epsilon^{3/2} \lambda_{a-} \hat{r}^* \hat{x}^\dagger \hat{z}), \tag{75}$$

$$\frac{d\hat{g}}{dT} = \rho_1 \lambda_+ \epsilon (\epsilon \hat{p} - \hat{g}\hat{r} + \mu_+ \epsilon (\epsilon \hat{p}^* - \hat{g}\hat{r}^*)) + \frac{\rho_1}{\rho_2} \lambda_{b-} (\hat{x}\hat{z} - \hat{g}), \tag{76}$$

$$\frac{d\hat{p}}{dT} = \lambda_- (\hat{g}\hat{r} - \epsilon \hat{p}) + \mu_+ (\hat{p}^* - \hat{p}), \tag{77}$$

$$\epsilon \frac{d\hat{p}^*}{dT} = \mu_-(\hat{p} - \hat{p}^*) + \theta_\mu \mu_- \lambda_- \epsilon (\hat{g}\hat{r}^* - \epsilon\hat{p}^*) + \frac{\lambda_{a-}}{\mu}\epsilon^{5/2}\hat{r}^*\hat{x}^\dagger\hat{z} - \lambda_{a+}\epsilon\hat{p}^*, \quad (78)$$

$$\frac{d\hat{x}}{dT} = \lambda_{g-}\epsilon^{3/2}(\epsilon\hat{x}^\dagger - \hat{x}) + \lambda_{b-}(\hat{g} - \hat{x}\hat{z}), \quad (79)$$

$$\frac{d\hat{x}^\dagger}{dT} = \rho_2\epsilon^{1/2}\frac{\lambda_{g+}\lambda_+}{\lambda_g - \lambda_-}(\mu\lambda_{a+}\hat{p}^* - \lambda_{a-}\epsilon^{3/2}\hat{r}^*\hat{x}^\dagger\hat{z}) + \lambda_{g+}(\hat{x} - \epsilon^{1/2}\hat{x}^\dagger), \quad (80)$$

$$\frac{d\hat{z}}{dT} = \rho_2\epsilon^2\frac{\lambda_{b+}\lambda_+}{\lambda_b - \lambda_-}(\mu\lambda_{a+}\hat{p}^* - \lambda_{a-}\epsilon^{3/2}\hat{r}^*\hat{x}^\dagger\hat{z}) + \lambda_{b+}(\hat{g} - \hat{x}\hat{z}). \quad (81)$$

Asymptotic analysis (with $\hat{r} = \hat{r}_0 + \epsilon^{1/2}\hat{r}_1 + \epsilon\hat{r}_2 + \cdots$, etc.) reveals the leading order problem

$$\frac{d\hat{r}_0}{dT} = \hat{r}_0^* - \hat{r}_0, \qquad \frac{d\hat{g}_0}{dT} = \frac{\rho_1}{\rho_2}\lambda_{b-}(\hat{x}_0\hat{z}_0 - \hat{g}_0), \quad \hat{r}_0 = \hat{r}_0^*, \quad (82)$$

$$\frac{d\hat{p}_0}{dT} = \lambda_-\hat{g}_0\hat{r}_0 + \mu_+(\hat{p}_0^* - \hat{p}_0), \quad \frac{d\hat{x}_0}{dT} = \lambda_{b-}(\hat{g}_0 - \hat{x}_0\hat{z}_0), \qquad \hat{p}_0^* = \hat{p}_0, \quad (83)$$

$$\frac{d\hat{x}_0^\dagger}{dT} = \lambda_{g+}\hat{x}_0, \qquad \frac{d\hat{z}_0}{dT} = \lambda_{b+}(\hat{g}_0 - \hat{x}_0\hat{z}_0). \quad (84)$$

Hence matching requires that

$$\hat{r}_0 = \hat{r}_0^* = r_e. \quad (85)$$

Linear combinations of (82) and (83), and of (83) and (84), give, again on matching. that

$$\hat{g}_0 + \frac{\rho_1}{\rho_2}\hat{x}_0 = g_e, \quad \lambda_{b+}\hat{x}_0 = \lambda_{b-}\hat{z}_0. \quad (86)$$

Substituting into Eq. (82) leads to the nonlinear equation

$$\frac{d\hat{g}_0}{dT} = \lambda_{b+}\frac{\rho_2}{\rho_1}(g_e - \hat{g}_0)^2 - \frac{\rho_1}{\rho_2}\lambda_{b-}\hat{g}_0. \quad (87)$$

with solution

$$\hat{g}_0 = \frac{2a_1}{1 + a_2 e^{2a_1\lambda_{b+}\frac{\rho_2}{\rho_1}T}} + g_e + \frac{\rho_1^2\lambda_{b-}}{\rho_2^2\lambda_{b+}} - a_1, \quad (88)$$

where

$$a_1 = \frac{\lambda_{b-}\rho_1}{\lambda_{b+}\rho_2}\sqrt{\frac{\rho_1^2}{\rho_2^2} + 4g_e\frac{\lambda_{b+}}{\lambda_{b-}}}, \quad a_2 = \frac{2\sqrt{1 + 4g_e\frac{\lambda_{b+}\rho_2^2}{\lambda_{b-}\rho_1^2}}}{\sqrt{1 + 4g_e\frac{\lambda_{b+}\rho_2^2}{\lambda_{b-}\rho_1^2}} - 1}. \quad (89)$$
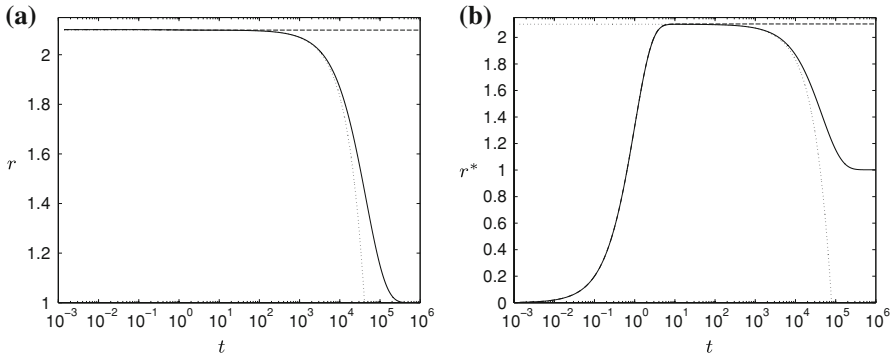
Fig. 16 Numerics (*solid*) and leading-order short- (dashed) and intermediate-time (*dotted*) asymptotics for **a** r; **b** r^*
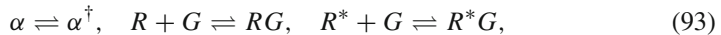
Hence, solutions for $\hat{x}_0$ and $\hat{z}_0$ can be easily calculated from Eq. (86). Further integration gives

$$\hat{p}_0 = \hat{p}_0^* = \lambda_- r_e \left(\frac{4a_1^2 \lambda_{b+} \frac{\rho_2}{\rho_1} a_2}{(1+a_2)^2} - \frac{4a_1^2 \lambda_{b+} \frac{\rho_2}{\rho_1} e^{2a_1 \lambda_{b+} \frac{\rho_2}{\rho_1} T}}{1 + a_2 e^{2a_1 \lambda_{b+} \frac{\rho_2}{\rho_1} T}} \right.$$
$$\left. + \left(g_e + \frac{\rho_1^2 \lambda_{b-}}{\rho_2^2 \lambda_{b+}} - a_1 \right) T \right), \tag{90}$$

$$\hat{x}_0^\dagger = \frac{\rho_2}{\rho_1} \lambda_{g+} \left(g_e T - \frac{1}{\lambda_- r_e} \hat{p}_0 \right), \qquad \hat{r}_1 = \hat{r}_1^* = 0, \tag{91}$$

$$\hat{x}_1^\dagger = \rho_2 \frac{\lambda_{g+} \lambda_+}{\lambda_g - \lambda_-} \mu \lambda_{a+} \hat{p}_0^* - \lambda_{g+} \hat{x}_0^\dagger \qquad \hat{r}_2 = \hat{r}_2^* = -\frac{\lambda_+}{\lambda_-} \hat{p}_0 - r_e, \tag{92}$$

The reaction that to leading order reaches equilibrium on this timescale is $\alpha + \beta\gamma \rightleftharpoons G$, whilst the reactions

$$\alpha \rightleftharpoons \alpha^\dagger, \quad R + G \rightleftharpoons RG, \quad R^* + G \rightleftharpoons R^*G, \tag{93}$$

are beginning to take effect. It is interesting to note that the leading order solutions for x and z correspond to the the peak numerical values in Fig. 18c, d. It can be seen from Eqs. (85), (91), (92), for r using (90) that the expansion disorders at $T = O(\epsilon^{-1})$ (i.e. $\tilde{t} = O(\epsilon^{-2})$)) (Figs. 16 and 17).

4.5 Long-time asymptotics : $t = O(\epsilon^{-2})$

This timescale corresponds in dimensional terms to times of order 10^3 s. The scalings are $\tau = \epsilon^2 t$ in Eqs. (46)–(53) with $x^\dagger = \epsilon^{-1/2} \check{x}^\dagger$, $r = \check{r}$, $r^* = \check{r}^*$, $g = \check{g}$, $p = \check{p}$,
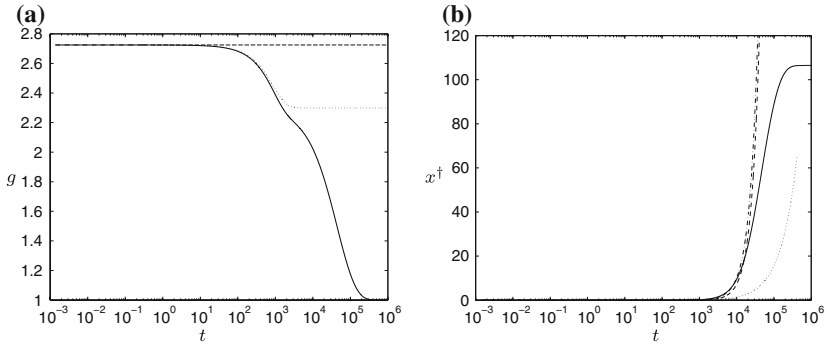
Fig. 17 Numerics (*solid*) and leading-order short- (*dashed*) and intermediate-time (*dotted*) asymptotics together with (*dot-dashed*) intermediate-time asymptotics including the first correction terms for **a** g; **b** $x^\dagger$
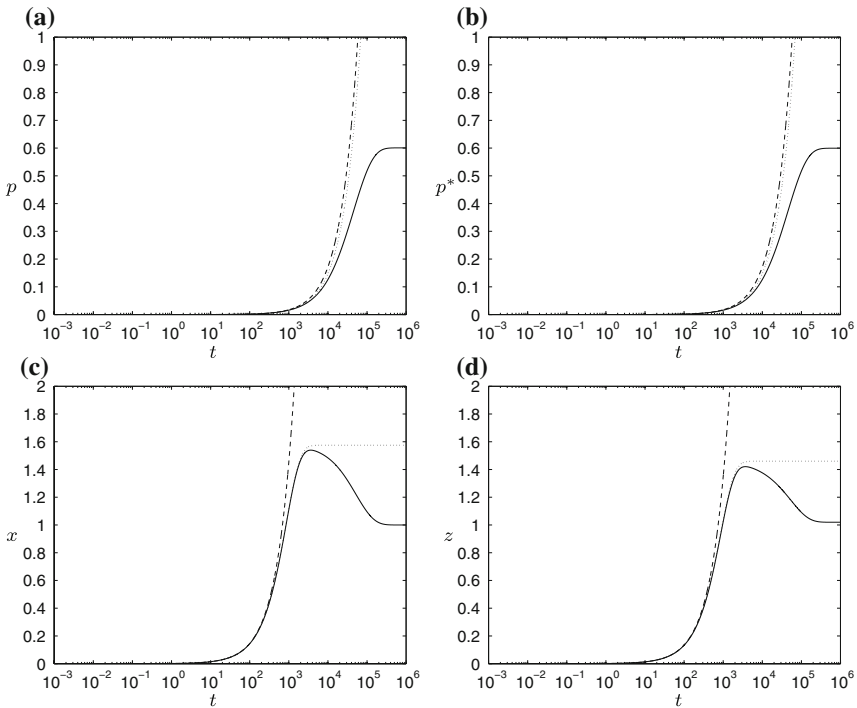
Fig. 18 Numerics (*solid*) and leading-order short- (*dashed*) and intermediate-time (*dotted*) asymptotics for **a** p; **b** p^*; **c** x; **d** z

$p^* = \check{p}^*$, $x = \check{x}$ and $z = \check{z}$, yielding

$$\epsilon \frac{\mathrm{d}\check{r}}{\mathrm{d}\tau} = \check{r}^* - \check{r} + \lambda_+ \epsilon (\check{p} - \check{g}\check{r}), \tag{94}$$

$$\epsilon^2 \frac{\mathrm{d}\check{r}^*}{\mathrm{d}\tau} = \check{r} - \check{r}^* + \theta_\mu \mu_+ \lambda_+ \epsilon^2 (\check{p}^* - \check{g}\check{r}^*) + \frac{\lambda_+}{\lambda_-} \epsilon (\mu \lambda_{a+} \check{p}^* - \lambda_{a-} \epsilon^{3/2} \check{r}^* \check{x}^\dagger \check{z}), \tag{95}$$

$$\epsilon \frac{d\check{g}}{d\tau} = \rho_1 \lambda_+ \epsilon (\check{p} - \check{g}\check{r} + \mu_+ \epsilon (\check{p}^* - \check{g}\check{r}^*)) + \frac{\rho_1}{\rho_2} \lambda_{b-} (\check{x}\check{z} - \check{g}), \tag{96}$$

$$\epsilon \frac{d\check{p}}{d\tau} = \lambda_- \epsilon (\check{g}\check{r} - \check{p} + \mu_+ (\check{p}^* - \check{p})), \tag{97}$$

$$\epsilon^2 \frac{d\check{p}^*}{d\tau} = \mu_- (\check{p} - \check{p}^*) + \theta_\mu \mu_- \lambda_- \epsilon^2 (\check{g}\check{r}^* - \check{p}^*)) + \frac{\lambda_{a-}}{\mu} \epsilon^{5/2} \check{r}^* \check{x}^\dagger \check{z} - \lambda_{a+} \epsilon \check{p}^*, \tag{98}$$

$$\epsilon \frac{d\check{x}}{d\tau} = \lambda_{g-} \epsilon (\check{x}^\dagger - \check{x}) + \lambda_{b-} (\check{g} - \check{x}\check{z}), \tag{99}$$

$$\epsilon^{1/2} \frac{d\check{x}^\dagger}{d\tau} = \rho_2 \frac{\lambda_{g+}\lambda_+}{\lambda_{g-}\lambda_-} (\mu\lambda_{a+} \check{p}^* - \lambda_{a-} \epsilon^{3/2} \check{r}^* \check{x}^\dagger \check{z}) + \lambda_{g+} (\epsilon^{1/2} \check{x} - \check{x}^\dagger), \tag{100}$$

$$\epsilon \frac{d\check{z}}{d\tau} = \rho_2 \epsilon \frac{\lambda_{b+}\lambda_+}{\lambda_{b-}\lambda_-} (\mu\lambda_{a+} \check{p}^* - \lambda_{a-} \epsilon^{3/2} \check{r}^* \check{x}^\dagger \check{z}) + \lambda_{b+} (\check{g} - \check{x}\check{z}), \tag{101}$$

Combinations of (94), (95) and (97), (98) (associated respectively with total numbers of unbound receptors and G-protein bound receptors)

$$\frac{d\check{r}}{d\tau} + \epsilon \frac{d\check{r}^*}{d\tau} = \lambda_+ \left(\check{p} - \check{g}\check{r} + \theta_\mu \mu_+ \epsilon \left(\check{p}^* - \check{g}\check{r}^* \right) \right) + \frac{\lambda_+}{\lambda_-} \left(\mu\lambda_{a+} \check{p}^* - \lambda_{a-} \epsilon^{3/2} \check{r}^* \check{x}^\dagger \check{z} \right), \tag{102}$$

$$\frac{d\check{p}}{d\tau} + \mu\epsilon \frac{d\check{p}^*}{d\tau} = \lambda_- \left(\check{g}\check{r} - \check{p} + \theta_\mu \mu_+ \epsilon \left(\check{g}\check{r}^* - \check{p}^* \right) \right) + \lambda_{a-} \epsilon^{3/2} \check{r}^* \check{x}^\dagger \check{z} - \lambda_{a+} \mu \check{p}^*, \tag{103}$$

Asymptotics again enable a largely explicit description of the behaviour of the nonlinear system (with $\check{r} = \check{r}_0 + \epsilon^{1/2}\check{r}_1 + \epsilon\check{r}_2 + \cdots$). The leading-order problem reads

$$\begin{aligned}
\frac{d\check{r}_0}{d\tau} &= \lambda_+ \left(\check{p}_0 - \check{g}_0\check{r}_0 \right) + \mu \frac{\lambda_+}{\lambda_-} \lambda_{a+} \check{p}_0, \\
\frac{d\check{p}_0}{d\tau} &= \lambda_- \left(\check{g}_0\check{r}_0 - \check{p}_0 \right) - \mu\lambda_{a+} \check{p}_0,
\end{aligned} \tag{104}$$

with

$$\check{r}_0 = \check{r}_0^*, \quad \check{p}_0 = \check{p}_0^*, \quad \lambda_{g+}\check{x}_0^\dagger = \rho_2 \frac{\lambda_+}{\lambda_-} \mu\lambda_{a+} \check{p}_0, \quad \check{g}_0 = \check{x}_0\check{z}_0. \tag{105}$$

Correction terms give

$$\frac{d\check{g}_0}{d\tau} = \rho_1 \lambda_+ (\check{p}_0 - \check{g}_0\check{r}_0) + \frac{\rho_1}{\rho_2} \lambda_{b-} (\check{x}_2\check{z}_0 + \check{x}_0\check{z}_2 - \check{g}_2), \tag{106}$$

$$\frac{d\check{x}_0}{d\tau} = \lambda_{g-}\check{x}_0^\dagger + \lambda_{b-} \left(\check{g}_2 - \check{x}_2\check{z}_0 - \check{x}_0\check{z}_2 \right), \tag{107}$$

$$\frac{d\check{z}_0}{d\tau} = \mu\rho_2 \frac{\lambda_{b+}\lambda_+}{\lambda_{b-}\lambda_-} \lambda_{a+} \check{p}_0 + \lambda_{b+} \left(\check{g}_2 - \check{x}_2\check{z}_0 - \check{x}_0\check{z}_2 \right). \tag{108}$$

Combining the equations in (105), and by matching with the intermediate-timescale results, we get

$$\check{r}_0 + \frac{\lambda_+}{\lambda_-}\check{p}_0 = r_e. \tag{109}$$

Similarly, we have

$$\check{g}_0 - \rho_1\check{r}_0 + \frac{\rho_1}{\rho_2}\frac{\lambda_{b-}}{\lambda_{b+}}\check{z}_0 = g_e - \rho_1 r_e, \quad \lambda_{b+}\check{x}_0 = \lambda_{b-}\check{z}_0, \tag{110}$$

and hence from (105)

$$\check{z}_0 = \sqrt{\frac{\lambda_{b+}}{\lambda_{b-}}\check{g}_0}, \tag{111}$$

where the positive root has been taken to maintain positivity. Thus we can write

$$\check{p}_0 = \frac{\lambda_-}{\lambda_+}(r_e - \check{r}_0), \tag{112}$$

$$\check{z}_0 = \frac{-\frac{\rho_1}{\rho_2} + \sqrt{\left(\frac{\rho_1}{\rho_2}\right)^2 - 4\frac{\lambda_{b+}}{\lambda_{b-}}\left(\rho_1 r_e - \rho_1\check{r}_0 - g_e\right)}}{2}, \tag{113}$$

Substituting for $\check{p}_0$ and $\check{g}_0$ in Eq. (105)a we get the (separable) first order nonlinear equation

$$\frac{\mathrm{d}\check{r}_0}{\mathrm{d}\tau} = (\lambda_- + \mu\lambda_{a+})\left(r_e - \check{r}_0\right)$$

$$- \frac{\lambda_+}{4}\check{r}_0\left(-\frac{\rho_1}{\rho_2}\sqrt{\frac{\lambda_{b-}}{\lambda_{b+}}} + \sqrt{\frac{\rho_1^2\lambda_{b-}}{\rho_2^2\lambda_{b+}} + 4\left(\rho_1\check{r}_0 - \rho_1 r_e + g_e\right)}\right)^2, \tag{114}$$

where $\check{r}_0(0) = r_e$, a problem that we solve numerically. The leading-order results, along with the intermediate-time asymptotics, are shown in Fig. 19. The species all tend to their equilibrium values, i.e. the remaining reactions

$$R + G \rightleftharpoons RG, \quad R^*G \rightleftharpoons R^* + \alpha^\dagger + \beta\gamma, \tag{115}$$

$$\alpha \rightleftharpoons \alpha^\dagger, \tag{116}$$
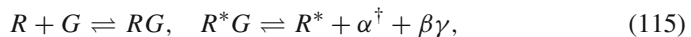
all equilibrate. The non-monotonicities in Fig. 19f, h are worth considering briefly. We saw in Sect. 4.3 that α and $\beta\gamma$ subunits were initially produced by the dissociation of G-protein in great quantities causing the levels to overshoot their final values. On this long time scale the reaction $G \rightleftharpoons \alpha + \beta\gamma$ is in equilibrium and so as the receptor binds to the G-protein and holds it in the RG complex, the amount of α and
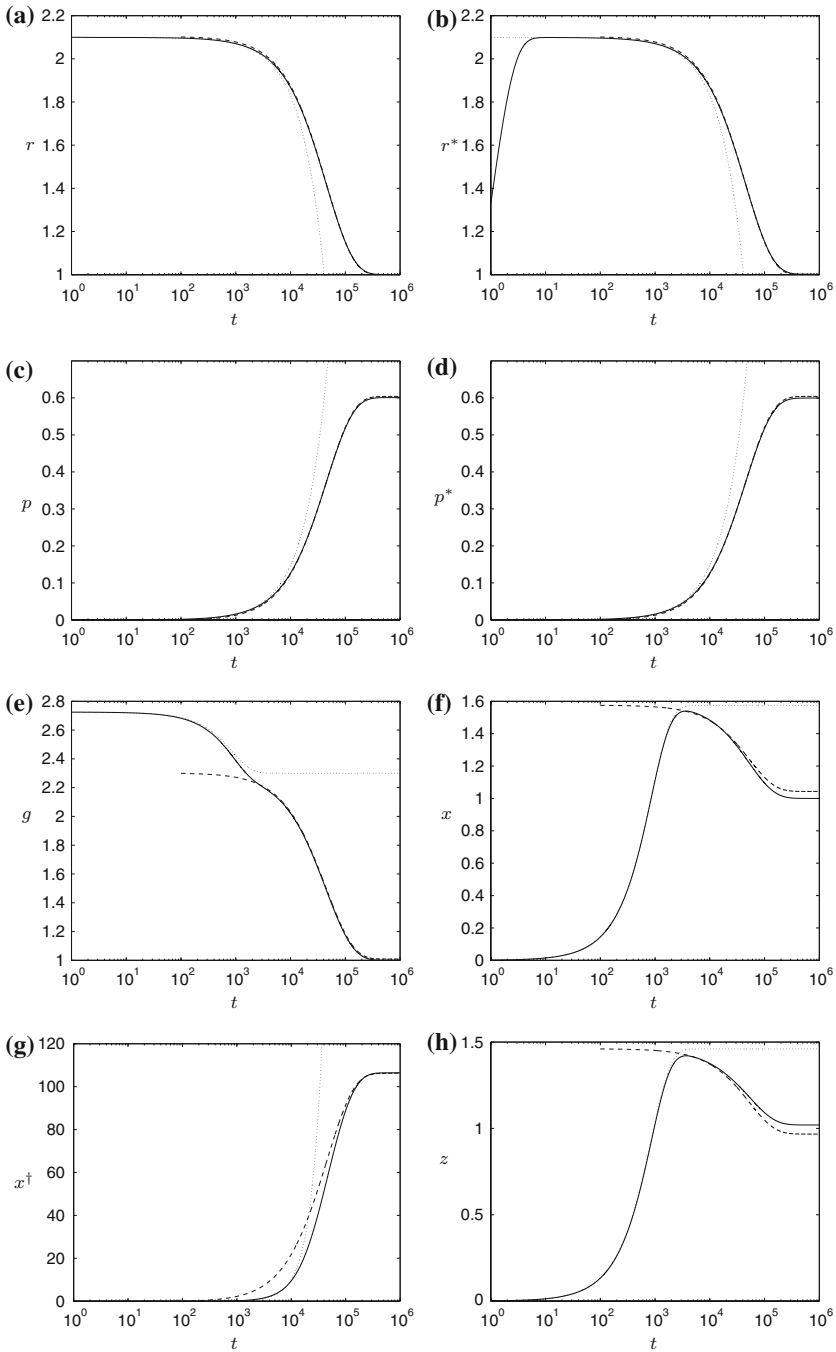
Fig. 19 Numerics (*solid line*), and intermediate-(*dotted*) and long-time (*dashed*) asymptotics for **a** r; **b** r^*; **c** p; **d** p^*; **e** g; **f** x; **g** $x^\dagger$; **h** z

$\beta\gamma$ subunits must decrease proportionally. Thus, we see the peak values drop down to lower plateaux.

5 Conclusions

The numerical solutions to the model were studied in the absence of drug. It is believed that drug-free analysis has not been performed in this much detail before, particularly with regard to the effects of forward and reverse reaction rates in the G-protein cycle on constitutive activity. The following conclusions were reached:

– The model behaves as expected in line with intuition from experiment (Shea et al. 2000), thus justifying it as a realistic model of the drug-free system.
– The model reflects that increasing the GTPase action (increasing k_{g+}) turns off the signal, also in line with intuition.
– It has been shown that increasing the propensity of the G-protein to bind to the activated receptor over the inactive form (modelled here by μ) demonstrates an increase in response.
– The model was used to demonstrate that constitutive receptor activation for $[\alpha^{\dagger}]$ and $[\beta\gamma]$ occurs, but is sensitive to parameters. In a future paper, this activation will be treated with inverse agonists to see if they turn the signal off.
– The percentage of receptors pre-coupled with G-protein increases with increasing k_+.

The model was also analysed asymptotically to give an idea of the dynamic behaviour:

– All the species move to equilibrium at similar rates $\sim 10^3$ s.
– In the first timescale (about one thousandth of a second), the main reaction is $[R] \rightleftharpoons [R^*]$, and so $[R]$ and $[R^*]$ reach equilibrium with each other. The concentrations of $[R]$, $[G]$ and $[\alpha]$ do not change much compared to their initial values. The other species all begin to be produced in small quantities compared to their equilibrium values. This timescale could be described as *receptor activation*.
– The intermediate timescale is of order one second. The main reaction is $[G] \rightleftharpoons [\alpha] + [\beta\gamma]$ which leads to the equilibrium for dissociation of the G-protein in the absence of receptor. This timescale could be described as *G-protein dissociation*.
– The last reactions that take place are $[R^*G] \rightleftharpoons [\alpha^{\dagger}] + [\beta\gamma] + [R^*]$, $[R] + [G] \rightleftharpoons [RG]$ and $[R^*] + [G] \rightleftharpoons [R^*G]$ which bring everything to equilibrium after about 1,000 s. This timescale could be described as *receptor-G-protein equilibration*.
– The activation reaction $[R^*G] \rightleftharpoons [\alpha^{\dagger}] + [\beta\gamma] + [R^*]$ forms the rate limiting step in G-protein activation.
– The mathematical analysis confirms the numerical results with an excellent match and establishes an approach which is equally effective in more general models.

However, it should be stressed that in our study of the drug-free shuttling mechanism the following aspects pertain.

- The initial conditions do not reflect a physiological possibility, but they were chosen to analyse how the system would move to equilibrium in order to determine which reactions dominate at different timescales.
- Some parameters were estimated since, although the current rate constant data available is relatively good, it is unfortunately not complete.

This paper builds on the work of Shea et al. (2000) by mathematically analysing a dynamic model of G-protein activation. It provides a background biology and introduction to the mathematics of G-protein cell signalling. To help confirm the accuracy of this model, it would be very useful to perform an experiment on constitutive receptor activation to try to match Figs. 8 and 10. While difficulties may arise in varying binding and activation rates and measuring $\alpha^\dagger$ and $\beta\gamma$ levels, varying receptor concentration should be possible. It is worth emphasizing again that experiments will not be possible to validate the dynamics of the system since any initial condition we choose is entirely artificial; the discussion of time courses does, however, give valuable insight into the time scales involved in G-protein activation.

The complexing model, which allows for the G-protein to remain bound to the receptor after activation, as mentioned by Kukkonen et al. (2001) and Chidiac (1998), was not analysed here, since insufficient parameter values could be found. The key reactions that would be operate are: $R^*G \rightleftharpoons R^*\alpha^\dagger + \beta\gamma$, $R^*\alpha^\dagger \rightleftharpoons R^*\alpha$ and $R^*\alpha + \beta\gamma \rightleftharpoons R^*G$.

This paper provides a solid basis for further exploration of the GPCR model, with the inclusion of ligand. The asymptotic approach demonstrates the dominant mechanisms for each timescale and this will be very useful when considering the more complex ligand-inclusive system.

Appendix

Rate constants and concentrations

The parameters were chosen to match those of Shea et al. (2000) where possible, since it provided the most complete set. In Table 1, the units for for each parameter are as for the value in the first column unless stated.

The three new parameters for which no information was known (k_{b-}, k_{g-} and k_{a-}) were estimated with values that would not change the equilibrium values significantly. (Note, k_{a-} appears to have a high value, but this is because it is the rate constant for a reaction in which three molecules have to come together, each of which is present in concentrations of $O(10^{-10} \text{ M})$.)

Equilibrium values

The equilibrium equations are derived by setting the left hand side to zero in equations (46)–(53),

Table 1 Dimensional parameter values

Param	Shea et al. (2000)	Riccobene et al. (1999)	Adams et al. (1998)	Leff et al. (1997)	Woolf et al. (2001)	Lemon et al. (2003)	This paper
k_p	1	10			2×10^{-5}		$1\,\mathrm{s^{-1}}$
k_q	$100 \to 1000$	10^5			10^6		$1000\,\mathrm{s^{-1}}$
k_f	$8.4 \times 10^7\,\mathrm{M^{-1}s^{-1}}$	$8.4 \times 10^7\,\mathrm{M^{-1}s^{-1}}$	8.4×10^7				$8.4 \times 10^7\,\mathrm{M^{-1}s^{-1}}$
k_r	$0.1 \to 10$	0.37	0.37				$0.37\,\mathrm{s^{-1}}$
k_+	$3 \times 10^{-8} \to 3 \times 10^{-4}\,(\mathrm{cell})^{-1}\mathrm{s^{-1}}$	10^{-7}	10^{-7}		10^{-5}		$3.6 \times 10^7\,\mathrm{M^{-1}s^{-1}}$
k_-	$3 \times 10^{-4} \to 3$				10^{-3}	0.017	$3 \times 10^{-3}\,\mathrm{s^{-1}}$
k_{b+}	$10^{-4}\,(\mathrm{cell})^{-1}\mathrm{s^{-1}}$				10^{-3}		$1.2 \times 10^{10}\,\mathrm{M^{-1}s^{-1}}$
k_{g+}	$0.1 \to 1$	0.2	0.2		0.01	0.15	$0.1\,\mathrm{s^{-1}}$
k_{a+}	$1 \to 5$						$1\,\mathrm{s^{-1}}$
k_{b-}							$0.144\,\mathrm{s^{-1}}$
k_{g-}							$10^{-4}\,\mathrm{s^{-1}}$
k_{a-}							$10^{18}\,\mathrm{M^{-2}s^{-1}}$
$[G_{TOT}]$	$10^4\,\mathrm{cell^{-1}}$	10^5	9.8×10^4		10^5	10^5	$4.15 \times 10^{-10}\,\mathrm{M}$
$[R_{TOT}]$	$10^4\,\mathrm{cell^{-1}}$	5.5×10^4	5.5×10^4		10^4	2×10^4	$4.15 \times 10^{-10}\,\mathrm{M}$
$[A]$	$10^{-11} \to 10^{-3}\,\mathrm{M}$	$10^{-12} \to 10^{-6}$	$10^{-10} \to 10^{-6}$		$10^{-9} \to 10^{-4}$		$10^{-12} \to 10^{-4}\,\mathrm{M}$
K_G	$10^{-4} \to 0.1$	10^{-4}			10		$10^{-4}\,\mathrm{M^{-1}}$
K_P	$10^{-3} \to 0.1$			$0.01 \to 5$	0.001		10^{-3}
K_A		$2.3 \times 10^8\,\mathrm{M}$	$2.3 \times 10^8\,\mathrm{M}$	$10^4 \to 10^{10}$		2×10^5	$2.3 \times 10^8\,\mathrm{M^{-1}}$
ζ	$10 \to 100$	$1 \to 10^6$			$0.01 \to 100$		10^3
μ	$10 \to 100$		3.57				2

Table 1 continued

Param	Shea et al. (2000)	Riccobene et al. (1999)	Adams et al. (1998)	Leff et al. (1997)	Woolf et al. (2001)	Lemon et al. (2003)	This paper
ν	$1 \to 10$				1		1
ζ_+	1	$1 \to 10^6$			$0.01 \to 100$		1
μ_+	1		3.57				1
ν_+	1				1		1
θ_ζ	1				1		1
θ_μ	$0.66 \to 6.6 \times 10^3$				1		1
θ_ν	1						1
$\theta_{\zeta\mu}$	1				1		1
$\theta_{\zeta\nu}$	1						1
$\theta_{\mu\nu}$	$0.3 \to 3 \times 10^3$				1		1
θ_a	1				1		1
$[cells]$			5×10^6				5×10^6

$$0 = r^* - r + \lambda_+ \epsilon (p - gr), \tag{117}$$

$$0 = r - r^* + \theta_\mu \mu_+ \lambda_+ \epsilon^2 (p^* - gr^*) + \frac{\lambda_+}{\lambda_-} \epsilon (\mu \lambda_{a+} p^* - \epsilon^2 \lambda_{a-} r^* x^\dagger z), \tag{118}$$

$$0 = \rho_1 \lambda_+ \epsilon (p - gr + \mu_+ \epsilon (p^* - gr^*)) + \frac{\rho_1}{\rho_2} \lambda_{b-} (xz - g), \tag{119}$$

$$0 = \lambda_- \epsilon (gr - p) + \mu_+ (p^* - p), \tag{120}$$

$$0 = \mu_- (p - p^*) + \theta_\mu \mu_- \lambda_- \epsilon^2 (gr^* - p^*) + \frac{\lambda_{a-}}{\mu} \epsilon^3 r^* x^\dagger z - \lambda_{a+} \epsilon p^*, \tag{121}$$

$$0 = \lambda_{g-} \epsilon^{3/2} (x^\dagger - x) + \lambda_{b-} (g - xz), \tag{122}$$

$$0 = \rho_2 \frac{\lambda_{g+} \lambda_+}{\lambda_{g-} \lambda_-} (\mu \lambda_{a+} p^* - \lambda_{a-} \epsilon^2 r^* x^\dagger z) + \lambda_{g+} \epsilon^{1/2} (x - x^\dagger), \tag{123}$$

$$0 = \rho_2 \epsilon^2 \frac{\lambda_{b+} \lambda_+}{\lambda_{b-} \lambda_-} (\mu \lambda_{a+} p^* - \lambda_{a-} \epsilon^2 r^* x^\dagger z) + \lambda_{b+} \epsilon (g - xz). \tag{124}$$

We also know from the analysis in Sect. 4.5 that the equilibrium value of $x^\dagger$ is $O(\epsilon^{-1/2})$. Therefore, we rescale $x^\dagger = \epsilon^{-1/2} \tilde{x}^\dagger$ to get

$$0 = r^* - r + \lambda_+ \epsilon (p - gr), \tag{125}$$

$$0 = r - r^* + \theta_\mu \mu_+ \lambda_+ \epsilon^2 (p^* - gr^*) + \frac{\lambda_+}{\lambda_-} \epsilon (\mu \lambda_{a+} p^* - \epsilon^{3/2} \lambda_{a-} r^* \tilde{x}^\dagger z), \tag{126}$$

$$0 = \rho_1 \lambda_+ \epsilon (p - gr + \mu_+ \epsilon (p^* - gr^*)) + \frac{\rho_1}{\rho_2} \lambda_{b-} (xz - g), \tag{127}$$

$$0 = \lambda_- \epsilon (gr - p) + \mu_+ (p^* - p), \tag{128}$$

$$0 = \mu_- (p - p^*) + \theta_\mu \mu_- \lambda_- \epsilon^2 (gr^* - p^*) + \frac{\lambda_{a-}}{\mu} \epsilon^{5/2} r^* \tilde{x}^\dagger z - \lambda_{a+} \epsilon p^*, \tag{129}$$

$$0 = \lambda_{g-} \epsilon (\tilde{x}^\dagger - \epsilon^{1/2} x) + \lambda_{b-} (g - xz), \tag{130}$$

$$0 = \rho_2 \frac{\lambda_{g+} \lambda_+}{\lambda_{g-} \lambda_-} (\mu \lambda_{a+} p^* - \lambda_{a-} \epsilon^{3/2} r^* \tilde{x}^\dagger z) + \lambda_{g+} (\epsilon^{1/2} x - \tilde{x}^\dagger), \tag{131}$$

$$0 = \rho_2 \epsilon \frac{\lambda_{b+} \lambda_+}{\lambda_{b-} \lambda_-} (\mu \lambda_{a+} p^* - \lambda_{a-} \epsilon^{3/2} r^* \tilde{x}^\dagger z) + \lambda_{b+} (g - xz). \tag{132}$$

Four leading order algebraic equations are thus

$$0 = r^* - r, \quad 0 = xz - g, \tag{133}$$

$$0 = p^* - p, \quad 0 = \rho_2 \frac{\lambda_+}{\lambda_{g-} \lambda_-} \mu \lambda_{a+} p^* - \tilde{x}^\dagger. \tag{134}$$

We can derive another relation by summing Eqs. (125) and (126) to get

$$0 = p - gr + \frac{\mu \lambda_{a+}}{\lambda_-} p^*. \tag{135}$$

Three more leading order algebraic equations can be derived from the conservation quantities described in Sect. 2.3. Equations (19)–(21) become

$$r_e = r + \epsilon r^* + \frac{\lambda_+}{\lambda_-} p + \mu \frac{\lambda_+}{\lambda_-} \epsilon p^*, \tag{136}$$

$$g_e = g + \rho_1 \frac{\lambda_+}{\lambda_-} p + \mu \rho_1 \frac{\lambda_+}{\lambda_-} \epsilon p^* + \epsilon^{1/2} \frac{\rho_1 \lambda_{g-}}{\rho_2 \lambda_{g+}} x^\dagger + \frac{\rho_1}{\rho_2} x, \tag{137}$$

$$\frac{\lambda_{b-}}{\lambda_{b+}} z = x + \epsilon^{1/2} \frac{\lambda_{g-}}{\lambda_{g+}} \tilde{x}^\dagger, \tag{138}$$

and so the leading order algebraic equations are

$$r_e = r + \frac{\lambda_+}{\lambda_-} p, \tag{139}$$

$$g_e = g + \frac{\rho_1}{\rho_2} x + \frac{\lambda_+}{\lambda_-} \rho_1 p, \tag{140}$$

$$z = \frac{\lambda_{b+}}{\lambda_{b-}} x. \tag{141}$$

Hence, the eight algebraic equations (133)–(135), (139)–(141) for the eight unknowns can be combined to form a quartic equation in x,

$$\frac{\lambda_+ \lambda_{b+}^2}{\lambda_- \lambda_{b-}^2} x^4 + \frac{\rho_1 \lambda_+ \lambda_{b+}}{\rho_2 \lambda_- \lambda_{b-}} x^3 + \frac{\lambda_{b+}}{\lambda_{b-}} \left(1 + \frac{\mu \lambda_{a+}}{\lambda_-} + \frac{\lambda_+ \rho_1 r_e}{\lambda_-} - \frac{\lambda_+ g_e}{\lambda_-} \right) x^2$$
$$+ \frac{\rho_1}{\rho_2} \left(1 + \frac{\mu \lambda_{a+}}{\lambda_-} \right) x - g_e \left(1 + \frac{\mu \lambda_{a+}}{\lambda_-} \right) = 0. \tag{142}$$

For the parameter set above the numerical values at equilibrium for these nondimensional variables are

$$r = 1, \qquad r^* = 1, \qquad g = 1, \qquad p = 0.6, \tag{143}$$
$$p^* = 0.6, \qquad x = 1, \qquad x^\dagger = 106.5, \qquad z = 1.02. \tag{144}$$

References

Adams JA, Omann GM, Linderman JJ (1998) A mathematical model for ligand/receptor/G-protein dynamics and actin polymerisation in human neutrophils. J Theo Biol 193:543–560

Alberts B, Bray D, Lewis J, Raff M, Roberts K, Watson JD (1994) Molecular biology of the cell. Garland Publishing, New York

Chen CY, Cordeaux Y, Hill SJ, King JR (2003) Modelling of signalling via G-protein coupled receptors: the pathway-dependent agonist potency and efficacy. B Math Biol 65:933–958

Chidiac P (1998) Rethinking receptor-G protein-effector interactions. Biochem Pharmacol 55:549–556

Clément F, Monniaux D, Stark J, Hardy K, Thalabard JC, Franks S, Claude D (2001) Mathematical model of FSH-induced cAMP production in ovarian follicles. J Physiol Endocrinol Metab 281:E35–E53

De Lean A, Stadel JM, Lefkowitz RJ (1980) A ternary complex model explains the agonist-specific binding properties of the adenylate cyclase-coupled β-adrenergic receptor. J Biol Chem 255:7108–7117

Fitzgerald LR, Manna IJ, Dytko GM, Wu H-L, Nambi P (1999) Measurement of responses from Gi-, Gs- or Gq-coupled receptors by a multiple response element/cAMP response element-directed reporter assay. Anal Biochem 275:54–61

Kenakin T (1993) Pharmacological analysis of drug-receptor interaction. Raven Press, New York

Kenakin T (1997) Molecular pharmacology. Blackwell Science, Oxford

Kenakin T (2001) Inverse, protean and ligand-selective agonism: matters of receptor conformation. FASEB 15:598–611

Kenakin T (2002) Drug efficacy at G protein-coupled receptors. Annu Rev Pharmacol Toxicol 42:349–379

Kinzer-Ursem TL, Linderman JJ (2007) Both ligand- and cell-specific parameters control ligand agonism in a kinetic model of G protein-coupled receptor signaling. PLoS Comput Biology 3:84–94

Krakauer DC, Page KM, Sealfon S (2002) Module dynamics of the GnRH signal transduction network. J Theo Biol 218:457–470

Kukkonen JP, Näsman J, Åkerman KEO (2001) Modelling of promiscuous receptor G_i/G_s protein coupling and effector response. TiPS 22:616–622

Leff P, Scaramellini C, Law C, McKechnie K (1997) A three-state receptor model of agonist action. TiPS 18:355–362

Lemon G, Gibson WG, Bennett MR (2003) Metatropic receptor activation, desensitization and sequestration–I: modelling calcium and inositol 1,4,5-triphosphate dynamics following receptor activation. J Theo Biol 223:93–111

Lidow MS, Roberts A, Zhang L, Koh P-O, Lezcano N, Bergson C (2001) Receptor crosstalk protein, calcyon, regulates affinity state of Dopamine D1 receptors. Eur J Pharmacol 427:187–193

Murray JD (1993) Mathematical biology. Springer, New York

Nauroschat J, ander Heiden U (1996) A theoretical approach to G-protein modulation of cellular responsiveness. J Math Biol 35:609–627

Riccobene TA, Omann GM, Linderman JJ (1999) Modeling activation and desensitization of G-protein coupled receptors provides insight into ligand efficacy. J Theo Biol 200:207–222

Shea L, Neubig R, Linderman J (2000) Timing is everything—the role of kinetics in G protein activation. Life Sci 68:647–658

Watson S, Arkinstall S (1994) The G-protein linked receptor factsbook. Academic Press Ltd, London

Woodroffe PJ, Bridge LJ, King JR, Hill SJ (2009) Modelling of the activation of G-protein coupled receptors by a single drug. Math Biosci (in press). doi:10.1016/j.mbs.2009.02.003

Woolf PJ, Kenakin TP, Linderman JJ (2001) Uncovering biases in high throughput screens of G-protein coupled receptors. J Theo Biol 208:403–418